


PAPER

[View Article Online](#)
[View Journal](#) | [View Issue](#)Cite this: *Dalton Trans.*, 2021, **50**,
2448Exploring the hyperpolarisation of EGTA-based
ligands using SABRE†Ben. J. Tickner, ^{‡§a} Yulia Borozdina,^{‡b} Simon B. Duckett ^{*a} and
Goran Angelovski ^{*b,c}

The design of molecules whose magnetic resonance (MR) signals report on their biological environment is receiving attention as a route to non-invasive functional MR. Hyperpolarisation techniques improve the sensitivity of MR and enable real time low concentration MR imaging, allowing for the development of novel functional imaging methodologies. In this work, we report on the synthesis of a series of EGTA-derived molecules (EGTA – ethylene glycol-bis(2-aminoethylether)-*N,N,N',N'*-tetraacetic acid), whose core structures are known to bind biologically relevant metal ions *in vivo*, in addition to pyridyl rings that allow reversible ligation to an iridium dihydride complex. Consequently, they are amenable to hyperpolarisation through the parahydrogen-based signal amplification by reversible exchange (SABRE) process. We investigate how the proximity of EGTA and pyridine units, and the identity of the linker group, affect the SABRE hyperpolarisation attained for each agent. We also describe the effect of catalyst identity and co-ligand presence on these measurements and can achieve ¹H NMR signal enhancements of up to 160-fold. We rationalise these results to suggest the design elements needed for probes amenable to SABRE hyperpolarisation whose MR signals might in the future report on the presence of metal ions.

Received 8th November 2020,
Accepted 21st January 2021

DOI: 10.1039/d0dt03839c

rsc.li/dalton

Introduction

Many spectroscopic techniques have been developed to study the chemical structures of molecules and the morphology of materials. These include the development of methods that rely on the principles of magnetic resonance (MR) to probe nuclear spin without the need for approaches based on ionising radiation such as X-ray, computed or positron emission tomography (CT or PET respectively), or sample destruction as in mass spectrometry. These advantages have led to magnetic resonance imaging (MRI) becoming routine for the diagnosis of structural abnormalities in living tissue.

Despite the diversity of its successes, MR is insensitive at the molecular level as the detected signal relies on small Boltzmann derived population differences across closely spaced nuclear spin energy levels. In fact, only around 1 in every 195 000 ¹H nuclei contribute positively to an MR signal recorded in a 1.5 T field common for clinical MRI scanners. It is not surprising therefore that MRI is usually concerned with detection of highly concentrated species, such as bulk water. Nevertheless, images with anatomical contrast can be produced by *T*₁ or *T*₂ weighted sequences to differentiate tissue morphologies. The information content of these approaches is often improved by the injection of a paramagnetic contrast agent.¹ However, as such images normally convey little direct information about biological function, there are opportunities to improve the diagnostic ability of MRI.

Many researchers are attempting to achieve this using biologically induced changes in the bulk water signal intensity.^{2,3} Among these are approaches such as functional MRI (fMRI), which attempts to probe the bulk water response as a function of the oxygenation state of haemoglobin,⁴ or chemical exchange saturation transfer (CEST), which modulates bulk water signals *via* proton exchange with an injected CEST agent.⁵ More recently, specific types of MRI contrast agents have been developed, being responsive to metal ions⁶ (Ca²⁺, K⁺, Mg²⁺, Zn²⁺, Fe²⁺, Fe³⁺, Cu²⁺ and others), neurotransmitters⁷ and proteins.⁸ The use of functional reporters that are able to

^aCentre for Hyperpolarisation in Magnetic Resonance (CHyM), Department of Chemistry, University of York, Heslington, York, YO10 5NY, UK.E-mail: simon.duckett@york.ac.uk^bMR Neuroimaging agents, Max Planck Institute for Biological Cybernetics, Tuebingen, 72076, Germany. E-mail: goran.angelovski@tuebingen.mpg.de^cLaboratory of Molecular and Cellular Neuroimaging, International Center for Primate Brain Research (ICPBR), Center for Excellence in Brain Science and Intelligence Technology (CEBSIT), Chinese Academy of Sciences (CAS), Shanghai, PR China

†Electronic supplementary information (ESI) available: Additional SABRE and NMR experiments. See DOI: 10.1039/d0dt03839c

‡These authors contributed equally to this work.

§Current address: NMR Research Unit, Faculty of Science, University of Oulu, P. O. Box 3000, 90014 Oulu, Finland.



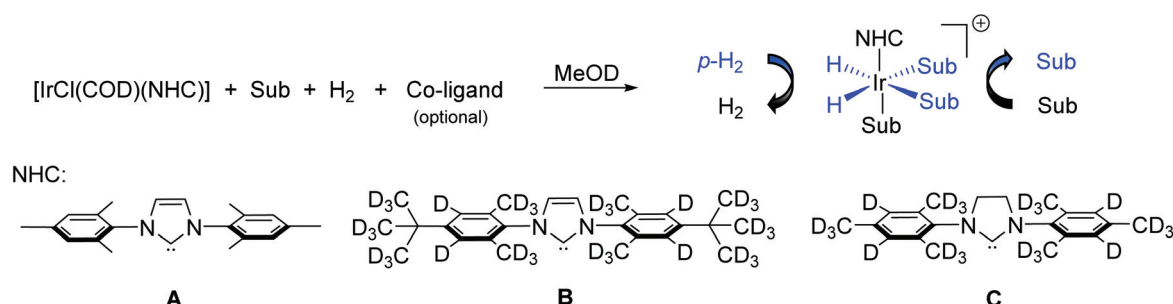
respond to such changes may therefore have benefit in studying different biological processes in a non-invasive way.

Approaches that target Ca^{2+} , both intracellular and extracellular, could have remarkable impact in neuroimaging due to the essential role of this ion in neuronal signalling.⁹ Other physiological processes that depend on Ca^{2+} could also be followed in real-time by means of MRI.¹⁰ For this approach to work, the preparation of appropriate functional markers is necessary and consequently, different types of Ca-responsive agents have been developed to date.^{11,12} Such reporters often consist of paramagnetic chelates coupled to a calcium sensing unit *via* a suitable linker.¹¹ Conformational changes in the agent upon metal ion binding are used to increase the inner sphere hydration of the paramagnetic ions, most commonly gadolinium, thereby enhancing the agent's relaxivity and subsequently increasing the intensity of the MRI signal in T_1 weighted images.¹²

While these functional imaging approaches have achieved great success, they do not fully address the low sensitivity of MRI. Over recent years, hyperpolarisation has been used to produce contrast agents with MR signals whose intensity is enhanced by up to five orders of magnitude relative to those derived from Boltzmann laws.¹³ With these hyperpolarised agents, successful imaging of low concentration biomolecules, drugs and metabolites *in vivo* was accomplished.^{13–15} While there are several possible experimental techniques for the production of hyperpolarised contrast agents, dissolution dynamic nuclear polarisation (d-DNP) has achieved the most success and a growing range of clinical applications are developing.¹³ However, d-DNP uses complex experimental apparatus to transfer polarisation from electrons to nuclei over a period of tens of minutes to several hours. The d-DNP procedure involves microwave irradiation of a target agent and organic radical in a 1–10 T field at temperatures between 1 and 5 K before rapid sample melting and transfer into the detection system.¹³ d-DNP hyperpolarisation has yielded ^{13}C polarisation levels of up to 70% for pyruvate-1- ^{13}C ¹⁴ and its subsequent metabolic imaging can identify cancer in humans *in vivo*.¹⁵

An alternative hyperpolarisation method uses parahydrogen ($p\text{H}_2$), the antisymmetric nuclear spin isomer of dihydrogen, as its source of polarisation. $p\text{H}_2$ reflects a potentially cheaper and faster route to a hyperpolarised contrast agent for *in vivo* injection and detection.¹⁶ Hydrogen gas exists as 25% $p\text{H}_2$ at room temperature with the remaining 75% consisting of ortho-hydrogen. H_2 can easily be enriched in the *para* state (>98%) by cooling to low temperature (28 K) in the presence of a spin exchange catalyst.¹⁷ While $p\text{H}_2$ is NMR silent, its latent hyperpolarisation is typically unlocked in a hydrogenation reaction.¹³ Consequently, $p\text{H}_2$ induced hyperpolarisation (PHIP) usually requires unsaturated functionality within the target agent.¹⁶ This can be alleviated by using a non-hydrogenative variant of PHIP, called signal amplification by reversible exchange (SABRE), which relies on a catalytic process to transfer $p\text{H}_2$ derived spin order to a target molecule.¹⁸ While SABRE is clearly at a much earlier stage in its development than DNP, the simplicity of this approach suggest that its potential clinical use is highly desirable. This can be highlighted by the fact that SABRE works in seconds by creating an iridium-based active polarisation transfer complex, which exchanges both $p\text{H}_2$ and a target substrate (Scheme 1).

Hyperpolarisation transfer is catalytic at low magnetic field (~65 G¹⁸ or 1–10 mG^{19,20} for transfer to ^1H or $^{13}\text{C}/^{15}\text{N}$ nuclei respectively) from the $p\text{H}_2$ derived hydride ligands in the catalyst to its bound target ligands through the associated J -coupling network. Subsequent ligand dissociation allows the build-up of chemically unchanged and yet hyperpolarised molecules in solution before their magnetisation decays slowly under relaxation back to the Boltzmann derived state. One of the most common substrates reported for hyperpolarisation using SABRE is the N-heterocycle pyridine and its derivatives.^{18,20–23} Indeed, pyridine was one of the first molecules to be hyperpolarised using SABRE¹⁸ and exhibits appropriate exchange kinetics to allow efficient polarisation transfer within the active $[\text{Ir}(\text{H})_2(\text{NHC})(\text{pyridine})_3]\text{Cl}$ catalyst, where NHC is an N-heterocyclic carbene.²⁴ SABRE has achieved up to 65% ^1H ,²² 4% ^{13}C ²⁵ and 79% ^{15}N ²⁶ polarisation for N-heterocycles, although other functionalities including



Scheme 1 SABRE involves the *in situ* formation of active polarisation transfer catalysts that reversibly exchange both $p\text{H}_2$ and substrate (Sub). Such species are typically of the type $[\text{Ir}(\text{H})_2(\text{NHC})(\text{Sub})_3]\text{Cl}$ where NHC is an N-heterocyclic carbene and are formed from the reaction of an iridium pre-catalyst with substrate and H_2 . Magnetisation is catalytically transferred from $p\text{H}_2$ derived hydride ligands to ligated substrate at an optimum magnetic field. Typical substrate molecules contain N-, O- or S-donor groups. In this work, Sub contains an iridium binding and EGTA-derived motif separated by a linker (Fig. 1). We also show the structures of the NHC ligands for the iridium precatalysts used in this work.



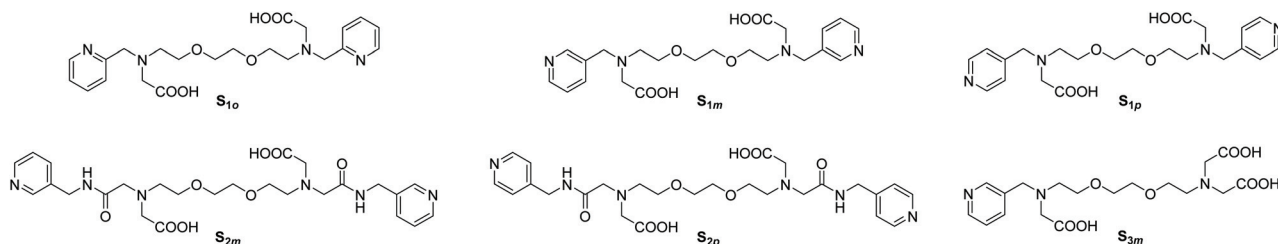


Fig. 1 Structures of the substrates used in this work. These contain Ca-binding chelators based on EGTA appended with pyridyl arms, which can bind iridium polarisation transfer catalysts used in SABRE hyperpolarisation.

nitriles,²⁷ amines²⁸ and even O-donors pyruvate¹⁹ and acetate²⁹ can be hyperpolarised by SABRE. Relayed proton exchange effects are now expanding the scope to include non-ligating molecules such as alcohols,³⁰ sugars³¹ and silanols.³² SABRE hyperpolarised molecules with MR signals responsive to factors such as pH^{33,34} NO concentration³⁵ or H₂O₂³⁶ have been reported.

Considering the importance that hyperpolarization techniques can have for the potential development of molecular fMRI approaches, in this work we aimed to combine the areas of bio-responsive MR probes and SABRE hyperpolarisation. Namely, we sought to explore SABRE on prototype responsive agents, which contain Ca-binding chelators appended with pyridyl units. Therefore, we report on the synthesis of several probes that contain functionalities based on ethylene glycol-bis(2-aminoethylether)-N,N,N',N'-tetraacetic acid (EGTA), which are known to ligate biologically relevant metal ions^{37,38} alongside pyridyl rings that can bind iridium as required for SABRE (Fig. 1).¹⁸ Moreover, we demonstrate the SABRE hyperpolarisation properties of the agents synthesised here and discuss a strategy for the rational design of responsive probes with enhanced MR signals.

Results and discussion

Design and synthesis of EGTA-based molecular probes suitable for SABRE hyperpolarisation

Development of Ca-sensitive hyperpolarized ¹³C and ¹⁵N contrast agents for MRI using the d-DNP technique has been reported recently.^{37,39,40} One of these hyperpolarisation approaches has been applied to ¹³C-EGTA, which is similar to the ligands used in this work. In this example, changes in hyperpolarised ¹³C-labelled carboxylate chemical shifts in response to coordination to various metals including calcium, magnesium and zinc were reported.³⁷ Here, we did not use ¹³C or ¹⁵N isotopically labelled molecules to improve the NMR signal, but functionalised EGTA, a typical calcium binding motif,³⁸ with pyridyl arms to create a series of molecules amenable to SABRE hyperpolarisation. This strategy of molecular functionalisation with a pyridyl group allowed us to create molecules compatible for SABRE hyperpolarisation and has been applied previously to fentanyl derivatives,⁴¹ synthetic oligopeptides⁴² and others.³⁵ The relative geometry of the

pyridyl binding site and the EGTA-derived unit is expected to play an important role in determining both metal sensitivity and SABRE efficiency. The steric properties of the target agents are particularly important in controlling binding affinity to iridium, as the hyperpolarisation of bulky ligands is known to be limited by steric repulsion between the catalyst and target agent.⁴³ Therefore, we prepared a set of agents that had *ortho* (*o*), *meta* (*m*) and *para* (*p*) relationships between the pyridyl nitrogen and the EGTA unit (Scheme 2).

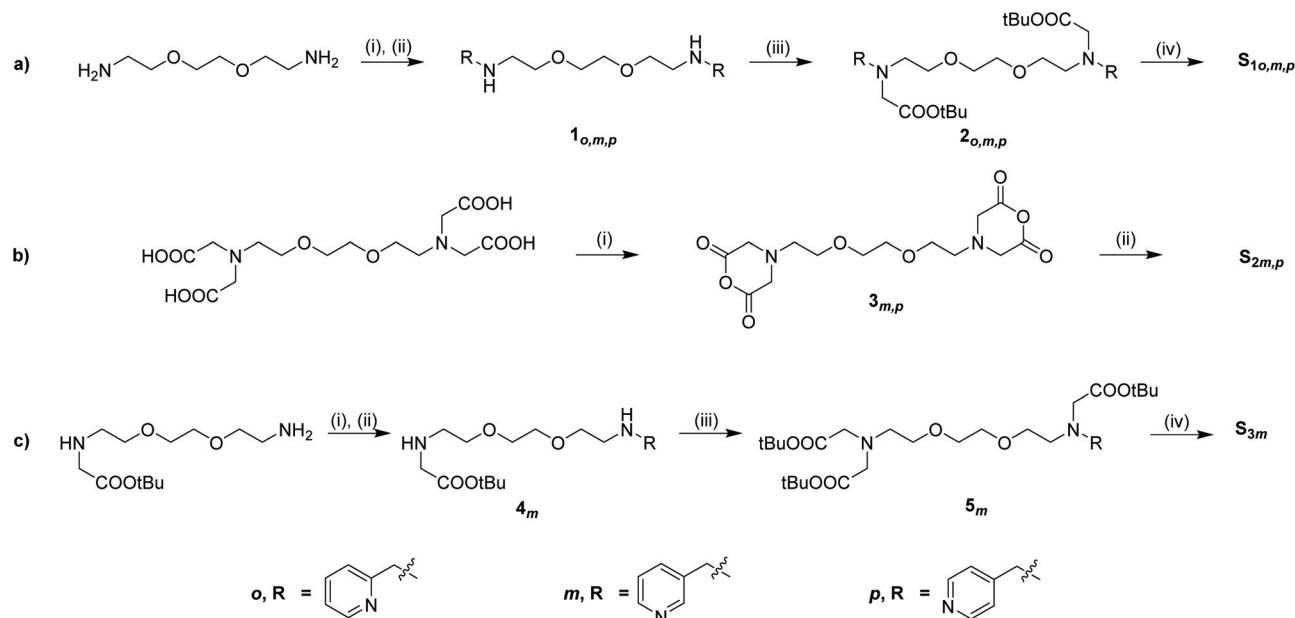
The synthesis of the desired products was performed in different 2- or 3-step procedures. Briefly, a reductive amination procedure was used to modify a 2,2'-(ethylenedioxy)bis(ethylamine) core with *ortho*-, *meta*-, or *para*-pyridinecarboxaldehydes in a step that proceeded quantitatively. The subsequent successive alkylation of the resulting pyridyl ethanamines, **1_{o,m,p}** with *tert*-butyl bromoacetate was tested using several reaction conditions. Reasonable yields of **2_{o,m,p}** were obtained in dry acetonitrile with the base potassium carbonate and potassium iodide. After their isolation and the subsequent acidic hydrolysis of the esters, the target substrates **S_{1m,p}** were crystallized by slow diffusion of methanol solutions into diethyl ether, while the acid derivative **S_{1o}** was isolated as a dark-red oil.

It has been reported that the substitution of two carboxylic groups by amide units in EGTA significantly influences its coordination properties and the consequent MR behaviour of the corresponding Gd-complexes.⁴⁴ Consequently, we also synthesised substrate **S₂** to investigate whether an amide group linking the pyridyl and EGTA units would have an effect on SABRE. **S₂** was synthesised in both *meta* (**S_{2m}**) and *para* (**S_{2p}**) forms in two steps by following a literature procedure with only minor modifications (Scheme 2b).⁴⁴ Finally, the substrate **S_{3m}**, which contains one pyridyl ring, was prepared in three steps (Scheme 2c). The hydrolysis step used conditions adapted from Zalupski *et al.*⁴⁵ The *ortho* isomer of **S₂** (**S_{2o}**) and the *ortho* and *para* derivatives of **S₃** (**S_{3o}** and **S_{3p}**, respectively) were not synthesised due to the prediction that they would exhibit poor SABRE or challenging synthetic preparation.

Formation of SABRE active complexes with substrates **S₁** and **S₂**

SABRE requires an active polarisation transfer catalyst that undergoes both pH₂ and substrate exchange.¹⁸ Typically, this





Scheme 2 Structures of (a) $\text{S}_{1o,m,p}$ (b) $\text{S}_{2m,p}$ and (c) S_{3m} , and a summary of their synthetic preparation: (a) (i) PyCHO, CH_2Cl_2 , N_2 ; (ii) NaBH_4 , EtOH, 0°C , N_2 ; (iii) $\text{BrCH}_2\text{COOtBu}$, K_2CO_3 , KI, DMF, N_2 ; (iv) TFA, CH_2Cl_2 , 0°C , N_2 (b) (i) Ac_2O , CH_2Cl_2 , N_2 ; (ii) PyNH_2 , Py (or Py/DMF), N_2 and (c) (i)–(iii) same as (a), (iv) HCl, dioxane, 0°C , N_2 .

is achieved by activating solutions containing $[\text{IrCl}(\text{COD})](\text{IMes})$, **A** where COD = *cis,cis*-1,5-cyclooctadiene and IMes = 1,3-bis(2,4,6-trimethyl-phenyl)imidazol-2-ylidene and 4–20 equivalents (relative to Ir) of substrate with 3 bar pH_2 in solvents such as methanol- d_4 or dichloromethane- d_2 . This process typically results in the formation of catalysts of the type $[\text{Ir}(\text{H})_2(\text{IMes})(\text{substrate})_3]\text{Cl}$, which then undergo the required ligand exchange processes needed for SABRE.¹⁸

The SABRE compatibility of substrates $\text{S}_{1o,m,p}$, $\text{S}_{2m,p}$ and S_{3m} was investigated by preparing samples of $[\text{IrCl}(\text{COD})(\text{IMes})]$ (**A**, 2.5 mM) and 4 equiv. of the substrate in 0.6 mL of methanol- d_4 . ^1H NMR spectra were then recorded at 298 K several hours after the addition of 3 bar H_2 . These measurements revealed in each case that hydride containing complexes form, but their signals were extremely weak indicating poor catalyst activation (Fig. S1, ESI†).

When the sample containing S_{1o} was shaken with 3-bar pH_2 for 10 seconds at 65 G, and then examined by high-field (9.4 T) NMR, PHIP enhanced hydride signals were visible at δ –20.56 and –31.21 (Fig. 2a). These signals are consistent with hydride environments *trans* to nitrogen- and oxygen-donor sites respectively. It is therefore likely that they arise from a complex of the type $[\text{Ir}(\text{H})_2(\text{IMes})(\kappa^2\text{-N,O-S}_{1o})(\text{L})]$, in which S_{1o} is bound through N- and O-sites. This is possible due to the *ortho* arrangement of the pyridyl ring and the carboxylate motif. Related complexes containing bidentate $\text{H}_2\text{NCH}_2\text{COO}^-$ and RNC(R)COO^- ligands have been reported with their hydride resonances yielding similar chemical shifts.^{46,47}

In contrast, when the same experiments were repeated using S_{1m} and S_{1p} , hyperpolarised hydride NMR signals for analogous $[\text{Ir}(\text{H})_2(\text{IMes})(\kappa^2\text{-N,O-S}_i)(\text{L})]$ complexes are no longer observed. This is likely the result of the arrangement between

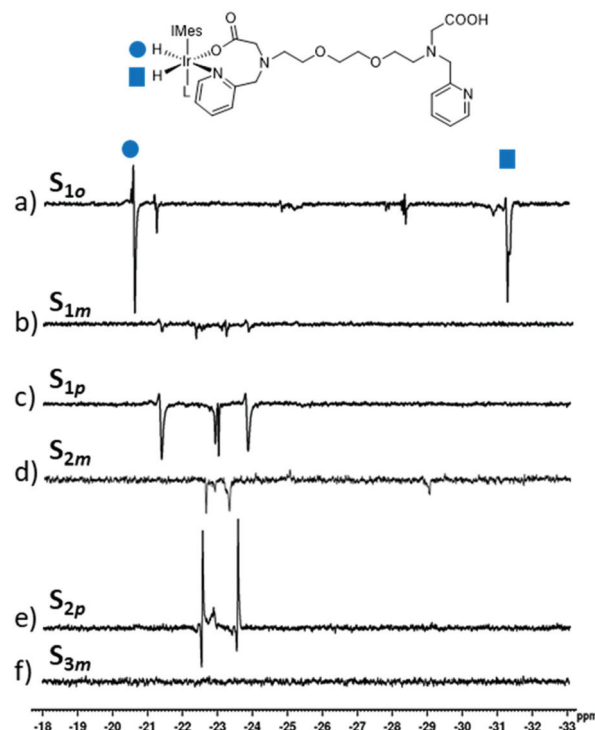


Fig. 2 Partial single scan ^1H NMR spectra recorded at 9.4 T and 298 K after a sample containing $[\text{IrCl}(\text{COD})(\text{IMes})]$ (2.5 mM) and 4 equiv. (a) S_{1o} (b) S_{1m} (c) S_{1p} (d) S_{2m} (e) S_{2p} and (f) S_{3m} in 0.6 mL of methanol- d_4 were shaken with 3 bar pH_2 for 10 seconds at 65 G.

the pyridyl ring and the EGTA unit leading to steric strain in such products. Consequently, S_{1m} and S_{1p} can no longer act as N,O-donors in the same way as S_{1o} . In the case of S_{1m} and S_{1p} ,



hyperpolarised signals at δ -21.30 and -23.79 are observed instead. For S_{2m} and S_{2p} , the corresponding hyperpolarised signals appear at δ -22.53 and -23.54 (Fig. 2d and e respectively). The chemical shifts of these signals are characteristic of hydride ligands lying *trans* to chloride^{19,48,49} or pyridyl nitrogen.^{21,22,26–28,43,50} Therefore, these ^1H NMR signals are expected to arise from $[\text{IrCl}(\text{H})_2(\text{IMes})(N\text{-}S_{1-2})(\text{L})]$ where L, located *cis* to hydrides and *trans* to the NHC, is expected to correspond to S_{1-2} . Full NMR characterisation and structural elucidation of these complexes was hampered by their low NMR signal intensity, which may reflect low stability. No PHIP enhanced hydride signals were observed using S_{3m} suggesting that in this case an active polarisation transfer catalyst is not formed. We attribute this to the large steric size of S_{3m} , which in this case would likely prevent binding of the two S_{3m} molecules necessary to form an analogous $[\text{IrCl}(\text{H})_2(\text{IMes})(N\text{-}S_{3m})(\text{L})]$ complex, where L is S_{3m} .

No NMR signal enhancements corresponding to the agents $S_{1o,m,p}$, S_{2p} or S_{3m} themselves are observed suggesting that while iridium-agent complexes exhibiting PHIP enhanced hydride resonances are formed using $S_{1o,m,p}$ and S_{2p} , these complexes do not act as SABRE polarisation transfer catalysts in these cases. In contrast, hyperpolarised ^1H NMR resonances for the pyridyl ring of S_{2m} were observed (Fig. 3b–d); the *ortho*

sites were enhanced by 16 and 13-fold relative to their Boltzmann derived signal strengths. The more distant *meta* and *para* ^1H NMR sites were enhanced by 9 and 12-fold respectively. The corresponding signal gains achieved at 273 K were comparable to these, although they increased to 32, 37, 12 and 21-fold for the two *ortho*, *meta* and *para* sites respectively at 318 K. This is likely to be the result of faster ligand exchange and suggests the resulting complex is reasonably stable.^{21,24}

Use of co-ligands to form stable SABRE active complexes

Agents S_{1-3} reflect some of the most structurally complex molecules investigated for hyperpolarisation using SABRE, which is usually applied to low molecular weight molecules with less than 20 atoms.²³ The large size of S_{1-3} is likely to hamper the formation of typical SABRE catalysts of the type $[\text{Ir}(\text{H})_2(\text{IMes})(S_{1-3})_3]\text{Cl}$. In previous studies using sterically large targets, substrate coordination can be favoured by using SABRE catalysts with sterically smaller carbene ligands.⁴³ The addition of a co-ligand to support the formation of active polarisation transfer catalysts with sterically large substrates³⁵ or weakly donating O-donor ligands has also been used.^{19,29} We therefore added the co-ligands acetonitrile^{27,51} or benzylamine^{26,28} to see if suitable stable polarisation transfer catalysts form with agents S_{1-3} .

The effect of acetonitrile was tested by its addition (0.5 μL , and then a further 2 μL) to solutions of preactivated $[\text{IrCl}(\text{COD})(\text{IMes})]$ (A, 2.5 mM) and S_1 (4 equiv.) with 3 bar H_2 in 0.6 mL of methanol- d_4 . No change in the appearance of the hydride region of the corresponding ^1H NMR spectra were observed when compared to the spectra observed without addition of this co-ligand (Fig. 2). This is surprising given the known stability of *mono*-substituted acetonitrile complexes of this type^{27,51} and supports our earlier hypothesis that the complexes formed in these cases likely do not undergo the ligand exchange needed for SABRE.^{18,23,24}

Therefore, as predicted, when a fresh sample was prepared containing A (4 mM), S_{1m} (3 equiv.), acetonitrile (2 equiv.) and 3 bar H_2 in 0.6 mL of methanol- d_4 , a different hydride-containing complex forms, exhibiting resonances at δ -20.77 and -22.29. These resonances are comparable to those previously reported for $[\text{Ir}(\text{H})_2(\text{IMes})(\text{NCCH}_3)(\text{pyridine})_2]\text{Cl}$, which appear at δ -20.56 and -22.12.²⁷ The formation of an analogous complex is supported by the observation of three sets of aromatic ^1H NMR resonances for three distinct types of pyridyl ring. The first of these has resonances at δ 8.79, 8.65, 7.62 and 8.17 and they match those of the free agent, S_{1m} . Additional sets of resonances at δ 8.43, 8.45, 7.25, 7.95 and δ 8.38, 8.72, 7.15, 7.85 are visible corresponding to the pyridyl groups of S_{1m} bound to iridium (Fig. 4b). 2D NMR characterisation data for this sample confirms the relative orientation of IMes, hydride, pyridyl and acetonitrile ligands in the immediate coordination sphere of the metal (Table S2 in ESI† for full characterisation details). These measurements cannot, however, confirm whether the two distinct bound pyridyl rings of S_{1m} arise from the same or separate molecules of bound

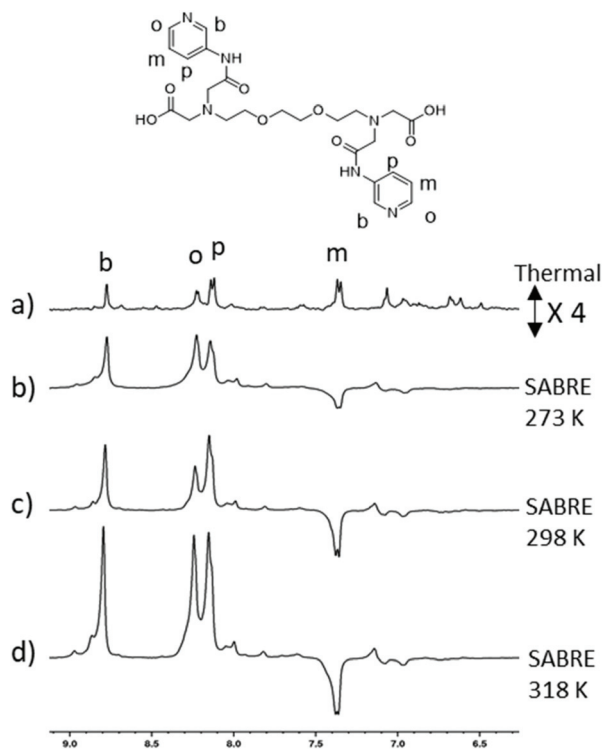


Fig. 3 Partial single scan ^1H NMR spectra of the aromatic region of a sample containing (a) thermally polarised $[\text{IrCl}(\text{COD})(\text{IMes})]$ (2.5 mM) and S_{2m} (4 equiv.) in 0.6 mL of methanol- d_4 (b)–(d) the same sample after shaking with 3 bar pH_2 at 65 G for 10 seconds after being left in a thermostatically controlled water bath at (b) 273 K (c) 298 K and (d) 318 K for 60 seconds prior to pH_2 shaking.



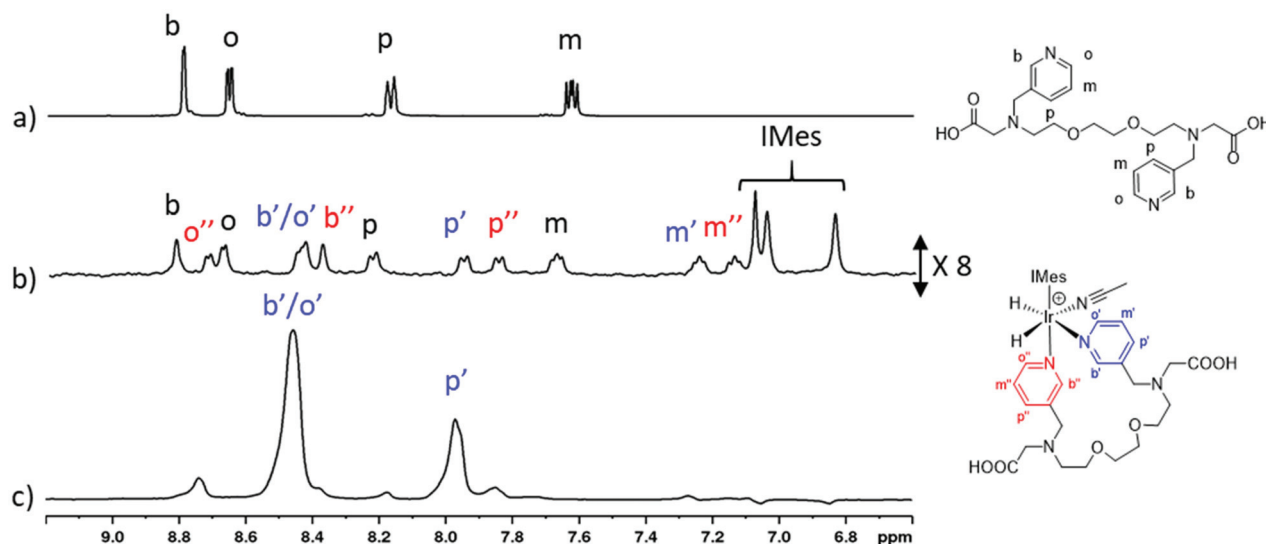


Fig. 4 (a) Signal averaged ^1H NMR spectrum of S_{1m} in 0.6 mL of methanol- d_4 recorded at 9.4 T and 298 K (b) partial single scan ^1H NMR spectrum of a sample containing $[\text{IrCl}(\text{COD})(\text{IMes})]$ (4 mM), S_{1m} (3 equiv.) and acetonitrile (2 equiv.) in 0.6 mL of methanol- d_4 recorded under Boltzmann conditions at 9.4 T and 298 K (c) SABRE hyperpolarised ^1H NMR spectrum after shaking the sample described in (b) with 3 bar pH_2 for 10 seconds at 65 G.

S_{1m} . We note that high resolution mass spectrometry did not yield molecular ion peaks corresponding to intact complexes due to severe molecular fragmentation, even with liquid injection field desorption ionization (LIFDI) techniques. However, the appearance of these bound aromatic ^1H NMR signals appears similar when an analogous sample is prepared using 0.9 equiv. of S_{1m} relative to catalyst (Fig. S6, ESI†). We therefore deduce the complex formed from S_{1m} is $[\text{Ir}(\text{H})_2(\text{IMes})(\text{NCCH}_3)(\kappa^2\text{-}N,N\text{-}\text{S}_{1m})]\text{Cl}$, in which S_{1m} acts as a bidentate ligand coordinating through both pyridyl rings. We note that when a sample of S_{3m} (4 equiv.) and **A** (2.5 mM) with 3 bar pH_2 in methanol- d_4 (0.6 mL) was prepared, no PHIP enhanced hydride containing complexes were formed, which suggests that both pyridyl rings of S_{1m} are required to form the hydride signals assigned as $[\text{Ir}(\text{H})_2(\text{IMes})(\text{NCCH}_3)(\kappa^2\text{-}N,N\text{-}\text{S}_{1m})]\text{Cl}$.

When such a sample containing S_{1m} was shaken for 10 seconds with pH_2 at 65 G, prior to recording a high-field ^1H NMR spectrum, the observed hydride resonances exhibit PHIP enhancement (Fig. S3, ESI†). To this end, some resonances in the aromatic region are now enhanced as a consequence of SABRE (Fig. 4). These hyperpolarised resonances correspond to one of the bound pyridyl rings in $[\text{Ir}(\text{H})_2(\text{IMes})(\text{NCCH}_3)(\kappa^2\text{-}N,N\text{-}\text{S}_{1m})]\text{Cl}$, which must occupy a binding site *trans* to hydride in order to receive polarisation transfer *via* SABRE.¹⁸ The ^1H NMR signal gains for the two *ortho* sites in this bound pyridyl ring (labelled as o and b in Fig. 4) are enhanced by a factor of 63-fold, compared to those recorded under Boltzmann derived conditions, although they cannot be distinguished from each other due to overlap. Signals for the *meta* and *para* sites in this pyridyl ring are enhanced by 3- and 53-fold respectively. Much weaker enhancements (<10-fold) are observed for a second set of resonances, which are attributed to a pyridyl ring that is

located *cis* to the hydride ligands of $[\text{Ir}(\text{H})_2(\text{IMes})(\text{NCCH}_3)(\kappa^2\text{-}N,N\text{-}\text{S}_{1m})]\text{Cl}$. Due to slow exchange, only a 3-fold enhancement is observed for the *para* resonance of the free agent. The NMR signal gains for each site have been compiled and summarized (Fig. 5 and Table S6 in ESI†).

When these SABRE measurements were repeated after leaving the sample in a water bath at 318 K for 60 seconds, prior to pH_2 shaking and detection at 298 K, the resulting ^1H NMR signal gains were roughly double those recorded when the shaking process was performed at 298 K (Fig. 5). In these measurements, NMR signal gains for the ^1H acetonitrile sites were also observed (enhanced by 27- and 48-fold per proton at 298 and 318 K respectively). A hyperpolarised ^{13}C NMR response for acetonitrile at δ 116 could also be discerned in a single scan when shaken in a mu-metal shield, while no enhanced ^{13}C signals corresponding to S_{1m} were visible (Fig. S4, ESI†). These enhanced acetonitrile signals are consistent with its dissociation from $[\text{Ir}(\text{H})_2(\text{IMes})(\text{NCCH}_3)(\kappa^2\text{-}N,N\text{-}\text{S}_{1m})]\text{Cl}$ providing a route to pH_2 exchange.^{27,52} These results suggest that in this system, an active SABRE catalyst of type $[\text{Ir}(\text{H})_2(\text{IMes})(\text{NCCH}_3)(\kappa^2\text{-}N,N\text{-}\text{S}_{1m})]\text{Cl}$ is able to catalyse polarisation transfer from pH_2 to S_{1m} . However, the high relative proportion of polarisation of S_{1m} bound to iridium suggests that exchange of this ligand is very slow.

The analogous polarisation transfer complex $[\text{Ir}(\text{H})_2(\text{IMes})(\text{NCCD}_3)(\kappa^2\text{-}N,N\text{-}\text{S}_{2m})]\text{Cl}$ forms when **A** (4 mM), S_{2m} (3 equiv.), acetonitrile- d_3 (2 equiv.) and 3 bar H_2 react in 0.6 mL of methanol- d_4 . However, when shaken with pH_2 at 298 K, ^1H NMR signal enhancements of less than 20-fold were seen for the corresponding bound ligand resonances, which did not improve at 273 or 318 K (see ESI, Table S3†). These signal gains for S_{2m} are comparable to those achieved in the absence



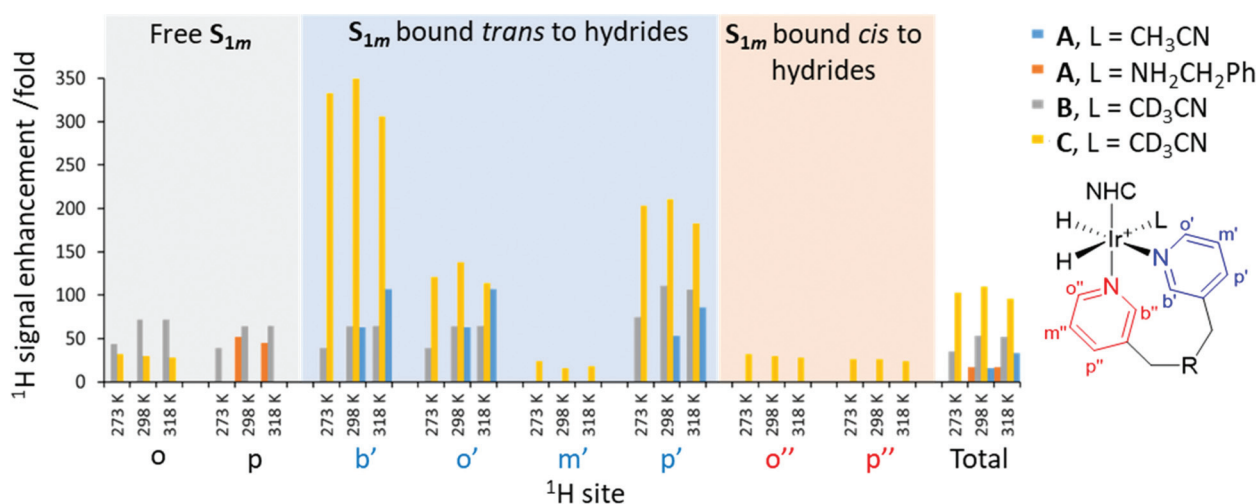


Fig. 5 SABRE ^1H NMR signal enhancements for $\text{S}_{1\text{m}}$ (3 equiv.) when shaken with precatalyst **A** (4 mM), the indicated co-ligand (2 equiv.) and 3 bar pH_2 in 0.6 mL of methanol- d_4 for 10 seconds at 65 G. For measurements recorded at 273 K and 318 K the samples were placed in a thermostatically controlled water bath for 60 seconds prior to pH_2 shaking and detection at 298 K. For individual sites, signal enhancements lower than 25-fold were omitted for clarity. A full table showing all signal enhancements for all sites, including errors, is given in the ESI Table S6.† Note that resonances omitted from the figure gave no signal enhancements. The structure of the NHC ligand and substrate $\text{S}_{1\text{m}}$ are shown in Scheme 1 and Fig. 1 respectively.

of a co-ligand. To improve the signal gains for these agents further an active polarisation transfer catalyst needs to be formed, which exchanges the target substrate more rapidly, whilst reducing polarisation wastage into the acetonitrile co-ligand.

Optimisation of SABRE enhancement of $\text{S}_{1\text{m}}$ by co-ligand and catalyst variation

The optimisation of SABRE performance is typically achieved by varying factors including the co-ligand^{50,53} and the carbene ligand of the catalyst,^{21,54} which serve to tune pH_2 and substrate exchange within the active catalyst. When analogous SABRE measurements were performed using samples containing **A** (4 mM), $\text{S}_{1\text{m}}$ (3 equiv.), and the known SABRE co-ligand benzylamine,^{26,28} a major hydride containing product is formed with signals at δ -22.25 and -22.80. This species is expected to correspond to the related $[\text{Ir}(\text{H})_2(\text{IMes})(\kappa^2\text{-}N,N\text{-}\text{S}_{1\text{m}})(\text{ND}_2\text{CH}_2\text{Ph})]\text{Cl}$; as whilst these measurements start with $\text{NH}_2\text{CH}_2\text{Ph}$, rapid H/D exchange in methanol- d_4 forms $\text{ND}_2\text{CH}_2\text{Ph}$.²⁸ When these samples were shaken with pH_2 , SABRE enhancements for the pyridyl groups of $\text{S}_{1\text{m}}$ bound within the catalyst were again observed; however, the effect is now much smaller than when acetonitrile was used as the co-ligand (Fig. 5). In these measurements, the presence of additional pyridyl resonances from the amine complicates spectral interpretation due to peak overlap. In fact, hyperpolarised signals for the pyridyl ring coordinated *cis* to hydrides are no longer discerned. In these cases, a more significant enhancement of the free *para* resonance of $\text{S}_{1\text{m}}$ is achieved (52-fold with benzylamine compared to 3-fold for acetonitrile), which does not increase at elevated temperatures.

Deuteration of ^1H sites in co-ligands, catalyst, or of target molecules, is often employed to optimise SABRE signal gains by preventing unwanted polarisation leakage and reducing relaxation.^{21,22} Catalyst design has also been used to fine tune substrate exchange rates with bulkier carbene ligands generally giving faster exchange.^{21,54} In order to encourage faster exchange of $\text{S}_{1\text{m}}$ within the active $[\text{Ir}(\text{H})_2(\text{NHC})\text{L}(\kappa^2\text{-}N,N\text{-}\text{S}_{1\text{m}})]\text{Cl}$ species, the bulkier iridium precatalysts **B** and **C** (Scheme 1) were used. Analogous samples were prepared containing **B** or **C** (4 mM), acetonitrile- d_3 (2 equiv.) and $\text{S}_{1\text{m}}$ (3 equiv.) with 3 bar H_2 in 0.6 mL of methanol- d_4 . Upon shaking mixtures containing precatalyst **B** with pH_2 at 298 K, total ^1H signal enhancements per proton for the pyridyl resonances of $\text{S}_{1\text{m}}$ free in solution and bound to the SABRE catalyst were estimated. These are now much higher at 49- and 43-fold, respectively, when compared to 3- and 26-fold, respectively, using catalyst **A** (see above). Similar increases relative to **A** were observed when catalyst **C** was used (total ^1H NMR signal enhancements per proton of 19- and 117-fold for free and bound $\text{S}_{1\text{m}}$, respectively). Interestingly, while precatalyst **B** gives the highest response for the free agent (an enhancement of 72-fold is observed for one of the free *ortho* sites), **C** gives higher signal gains for the bound agent (signal enhancements of 350-, 138- and 211-fold were observed for the two *ortho* and *para* pyridyl sites of $\text{S}_{1\text{m}}$ bound *trans* to the hydrides in the SABRE polarisation transfer catalyst, respectively). This suggests that the use of precatalysts **B** and **C** can yield more efficient SABRE hyperpolarisation of $\text{S}_{1\text{m}}$ relative to **A**. This is likely the effect of incorporation of the deuterium labels, which are expected to reduce relaxation in the active catalyst.²² The greater proportion of polarisation on the bound ligand using **C** suggests that polarisation transfer or hydrogen



Table 1 Summary of the highest ^1H NMR signal gains for these agents achieved using SABRE and the polarisation conditions. See ESI† for full structures of the agents, site labels and full tables of signal gains for all sites

Agent (3 equiv.)	Conditions			^1H NMR signal enhancements/fold			
	Catalyst (4 mM)	Co-ligand (2 equiv.)	T/K	Total free enhancement	Total bound enhancement	Highest enhancement for individual free site	Highest enhancement for individual bound site
S_{1o}	C	CD ₃ CN	318	25 ± 3	0	30 ± 2 (<i>o</i>)	0
S_{1m}	B	CD ₃ CN	298	49 ± 3	43 ± 3	72 ± 3 (<i>o</i>)	111 ± 6 (<i>p'</i>)
S_{1m}	C	CD ₃ CN	298	19 ± 1	117 ± 6	30 ± 1 (<i>o</i> , overlaps with <i>o''</i>)	350 ± 21 (<i>b'</i> or <i>o'</i>)
S_{1p}	C	CD ₃ CN	273	127 ± 19	0	159 ± 20 (<i>o</i>)	0
S_{2m}	C	None	318	33 ± 5	0	45 ± 8 (<i>b</i>)	0
S_{2p}	C	CD ₃ CN	298	5 ± 1	77 ± 3	5 ± 1 (<i>o</i>)	124 ± 6 (<i>o'</i>)
S_{3m}	C	CD ₃ CN	298	0	0	0	0

exchange within **C** is more efficient, but that relaxation or substrate exchange effects are less optimal compared to **B**. These signal gains are summarised in Fig. 5 and Table 1 (the Table S6 in ESI† contains a full table of signal enhancements).

Comparison of SABRE efficiency of S₁₋₃

Signal enhancements of **S_{1o}**, **S_{1p}**, **S_{2p}** and **S_{3m}** were also recorded under the same conditions as those which gave the highest signal enhancements for **S_{1m}**. This involved shaking samples containing precatalyst **C** (4 mM), acetonitrile-*d*₃ (2 equiv.) and substrate (3 equiv.). SABRE performance of **S_{2m}** (3 equiv.) was tested for a sample containing **C** (4 mM) with 3 bar p_{H2} in methanol-*d*₄ (0.6 mL). No co-ligand was used in this case as our previous tests (see above) found comparable signal enhancements for conditions with and without acetonitrile for this agent. Under these conditions, precatalyst **C** delivers 45-fold ^1H NMR signal gain for one of the *ortho* sites of free **S_{2m}** at 318 K (Table 1) which is slightly higher than the largest signal gain (37-fold) for the equivalent site at the same temperature using precatalyst **A** (2.5 mM).

For the remaining agents that were tested in the presence of acetonitrile-*d*₃, total hyperpolarised ^1H NMR responses for the free agent **S_{1o}** are 20-fold. Interestingly, the hydride region of these NMR spectra reveal the presence of PHIP enhanced signals at δ -20.16, -20.75, -28.58 and -31.31 (Fig. S21, ESI†). This result suggests that even in the presence of this co-ligand, **S_{1o}** can bind through both *N* and *O* sites to likely form $[\text{Ir}(\text{H})_2(\text{IMes})(\kappa^2\text{-N}, \text{O-S}_{1o})(\text{CH}_3\text{CN})]$, which may hamper its SABRE efficiency.

Interestingly, **S_{1p}** performs well under these conditions as the *ortho* and *meta* ^1H NMR resonances of the free agent are enhanced at 298 K by 138- and 68-fold respectively. These signal gains are higher than those achieved under analogous conditions for **S_{1m}** free in solution (corresponding sites <30-fold). ^1H NMR signal enhancements can be increased to 159- and 92-fold for the *ortho* and *meta* resonances, respectively, for free **S_{1p}** when polarisation transfer takes place at 273 K. A summary of these ^1H NMR signal gains is presented in Table 1 (a full table showing the NMR signal gains for each site is presented in the Table S8 in ESI†). There are no visible hyperpolarised signals for **S_{1p}** bound to the catalyst, which suggests that polarisation transfer efficiency or hydrogen exchange

using catalyst **C** must be less efficient for **S_{1p}** compared to using agent **S_{1m}**.

In contrast, SABRE ^1H NMR signal gains for free **S_{2p}** were low (<10-fold for the *ortho* site). Enhancements for the bound ligand were much higher at 77-fold suggesting that in this case polarisation transfer and ligand exchange processes are less efficient in comparison to **S_{1m}** and **S_{1p}**. The presence of a dominant PHIP enhanced hydride product at δ -20.9 and -22.2 appears when **S_{1m}**, **S_{1p}**, or **S_{2p}** are used (Fig. S21, ESI†), which suggests that these differences in SABRE efficiency for each agent are not due to a change in the identity of the active magnetisation transfer catalyst.

We also note that tests involving the mono-pyridyl containing agent, **S_{3m}**, did not yield discernible signals for any hydride containing complexes and no enhanced ^1H NMR signals were observed. This suggests that while the presence of two pyridyl rings in agents **S₁₋₂** may lead to slow exchange kinetics, it appears that both pyridyl rings in the sterically large agents reported in this work are important for ligation to form SABRE active complexes.

Conclusions

In this work we prepared and studied a series of novel agents that contain a pyridyl ring to allow hyperpolarisation using SABRE and a metal ligating unit derived from EGTA. The introduction of the pyridyl motif allows the prepared agents to coordinate to the iridium SABRE polarisation transfer catalyst. The hydride ligands of the resultant complexes were enhanced by parahydrogen and in the case of agent **S_{2m}** up to 33-fold enhancement is achieved for ^1H sites of the free pyridyl ring.

SABRE active complexes of the form $[\text{Ir}(\text{H})_2(\text{NHC})(\text{NCCH}_3)(\kappa^2\text{-N}, \text{N-S}_{1-2})]\text{Cl}$ can be formed using agents **S_{1m}**, **S_{1p}**, and **S_{2p}** when acetonitrile was used as a co-ligand. We find that ^1H NMR signal gains of **S_{1m}** can be increased by using bulkier catalysts and in some cases increasing the temperature to encourage substrate exchange and deuteration of the catalyst and co-ligand to reduce polarisation wastage. ^1H NMR signal gains of 72-fold for the *ortho* pyridyl site of free **S_{1m}** can be achieved using precatalyst **B**, although higher ^1H NMR signal gains of up to 350-fold can be achieved for pyridyl sites bound to pre-



catalyst C. We find that in many cases ^1H NMR signal gains for agents bound to the catalyst were much higher than those free in solution, which indicates slow ligand exchange and is perhaps expected given the large nature of these ligands and their ability to act as bidentate donors. Nevertheless, the molecules tested here reflect some of the sterically largest targets to be hyperpolarised using SABRE and ^1H NMR signal gains of up to 159-fold are observed for the *ortho* pyridyl sites of S_{2m} free in solution. We note that, to the best of our knowledge, the largest molecules successfully hyperpolarised using SABRE have molecular masses of 337 Da,⁴¹ and ~ 320 Da,^{35,42} both lower than the molecules reported in this work (<471 Da).

Furthermore, this work presents a rational to design functional molecules that can be hyperpolarised using SABRE. The obtained results indicate that an *ortho* relationship between the pyridyl nitrogen atom and the EGTA unit should be avoided, as agents with this steric arrangement can act as mixed N,O- donors to form $[\text{Ir}(\text{H})_2(\text{IMes})(\kappa^2\text{-N,O-S}_{10-20})(\text{L})]$ with reduced SABRE activity, even in the presence of a co-ligand. For the large substrates presented in this work, it appears the presence of two pyridyl rings is necessary for SABRE, as *mono*-pyridyl containing S_{3m} was not found to form any PHIP or SABRE active iridium adducts. We therefore highlight the tension between inclusion of iridium ligating groups to form SABRE active complexes, and labile exchange kinetics. We find no inherent significant difference in SABRE efficiency of *meta* (S_{1m} , S_{2m}) or *para* (S_{1p} , S_{2p}) substituted agents, which is consistent with other studies.⁴² Generally, higher ^1H NMR signal gains for agents $\text{S}_{1m,p}$ compared to $\text{S}_{2m,p}$ suggest that the increase in agent size upon inclusion of an additional amide linker group is not advantageous for SABRE hyperpolarisation.

However, it should be concluded that SABRE efficiency for all substrates strongly varies due to their various structural, as well as coordination, properties and exchange rates with the SABRE catalyst. Therefore, it is likely that different polarisation conditions (catalyst, co-ligand, concentration *etc.*) will have to be applied for each agent; this would require further optimisation, including increased pH_2 pressure or the use of related catalysts that have recently allowed the coordination of sterically larger^{43,50} or weakly coordinating^{19,29} substrates to increase the NMR signal gain. Removal of the SABRE catalyst will be required before any *in vivo* applications; the routes for its separation,^{55,56} and the development of water soluble catalysts, have already been reported.⁵⁷ Parallel progress in these areas will be required to produce a wider range of molecules whose MR signal(s) can respond to biological conditions. Consequently, the application of SABRE hyperpolarisation to address emerging molecular imaging questions could become feasible in the future.

Experimental section

General remarks

Materials. 2,2'-(Ethylenedioxy)bis(ethylamine) was purchased from TCI Europe (Zwijndrecht, Belgium). *tert*-Butyl (2-

(2-(2-aminoethoxy)ethoxy)ethyl)carbamate was purchased from Fisher Scientific (Germany). Ethylene glycol-bis(β -aminoethyl ether)-*N,N,N',N'*-tetraacetic acid, pyridinecarboxaldehydes, other chemicals and solvents were purchased from Merck (Sigma-Aldrich). The chemicals were used as received unless otherwise stated. Column chromatography was performed using silica gel 60 (0.03–0.2 mm) from Carl Roth (Germany). Low resolution mass spectra were recorded on an ion trap SL 1100 system Agilent with an electrospray ionization source. High resolution mass spectra were recorded on a Bruker Daltonics APEX II (FT-ICR-MS) with an electrospray ionization source. NMR characterization of S_{1-3} , and synthetic precursors, was performed on a 300 MHz Bruker Avance spectrometer, while all other NMR measurements were carried out on a 400 MHz Bruker Avance III spectrometer using solutions at room temperature (298 K) unless otherwise stated. Processing of NMR spectra was performed using TopSpin (Bruker GmbH) and ACD/SpecManager 9.0 (Advanced Chemistry Development, Inc.) software.

General procedure for reductive amination to form 1

2,2'-(Ethylenedioxy)bis(ethylamine) (13.5 mmol) was placed into a Schlenk flask with activated molecular sieves (3 Å) under a stream of nitrogen. Dry CH_2Cl_2 (15 mL) was added *via* a rubber septum. To the resulting solution, a pyridinecarboxaldehyde (28.3 mmol, 2.1 equiv.) was added dropwise. The flask was sealed with parafilm and the mixture was left stirring at room temperature under nitrogen for 18–20 h. The progress of the reaction was monitored by mass spectrometry and TLC analysis. After the reaction was completed, the mixture was filtered through a Celite layer and the solvent was distilled on a rotary evaporator until dry.

The flask with the residue was flushed with nitrogen and dry EtOH (15 mL) was added. The mixture was cooled in an ice bath. To the resulting solution, sodium borohydride (56.7 mmol, 4.2 equiv.) was added in portions. After stirring for ~ 1 hour, the ice bath was removed and the mixture was left stirring at room temperature overnight. The mixture was filtered through a glass filter and the solvent was evaporated. The residue was washed with water, extracted with CH_2Cl_2 (5–6 \times 40 mL), and dried over sodium sulfate. The inorganic salt was filtered, solvent evaporated, and the oily product dried on a high-vacuum pump. The purity of the so-obtained precursors 1 (according to NMR analysis) was found appropriate to continue without additional purification.

***N,N'*-(2-Pyridylmethyl)(ethylenedioxy)bis(ethylamine) (1_o).** The product was obtained as yellow oil in 89% yield. The spectroscopic characteristics were in agreement with the previously reported data.⁵⁸ ^1H NMR (CDCl_3) δ 2.83–2.86 (t, J = 5.2 Hz, $\text{CH}_2\text{-NH}$, 4H), 3.61–3.68 (m, O-CH_2 , 8H), 3.96 (s, $\text{O-CH}_2\text{-CH}_2\text{-NH}$, 4H), 7.14–7.18 (t, J = 6.14 Hz, $(\text{C-CH-CH})_{\text{py}}$, 2H), 7.34–7.37 (d, J = 7.74 Hz, $(\text{C-CH-CH})_{\text{py}}$, 2H), 7.61–7.67 (td, J_1 = 7.55 Hz, J_2 = 1.70 Hz, $(\text{N-CH-CH})_{\text{py}}$, 2H), 8.53–8.54 (d, J = 4.15 Hz, $(\text{N-CH-CH})_{\text{py}}$, 2H). ^{13}C NMR (CDCl_3) δ 48.6 ($\text{O-CH}_2\text{-CH}_2\text{-NH}$), 54.7 ($\text{CH}_2\text{-NH}$), 70.2 ($\text{O-CH}_2\text{-CH}_2\text{-NH}$, O-CH_2), 122.1 ($(\text{N-CH-CH})_{\text{py}}$).



$\text{CH})_{\text{Py}}$), 122.5 ((C-CH-CH) $_{\text{Py}}$), 136.6 ((C-CH-CH) $_{\text{Py}}$), 149.2 ((N-CH-CH) $_{\text{Py}}$), 158.9 ((CH-C-N) $_{\text{Py}}$).

***N,N'*-(3-Pyridylmethyl)(ethylenedioxy)bis(ethylamine) (1_m).** The product was obtained as orange oil in 93% yield. ^1H NMR (CDCl_3) δ 2.77–2.81 (t, J = 5.2 Hz, $\text{CH}_2\text{-NH}$, 4H), 3.58–3.62 (m, O-CH_2 , 8H), 3.80 (s, $\text{O-CH}_2\text{-CH}_2\text{-NH}$, 4H), 7.21–7.26 (dd, J_1 = 4.91 Hz, J_2 = 2.83 Hz, (C-CH-CH) $_{\text{Py}}$, 2H), 7.66–7.69 (d, J = 7.93 Hz, (C-CH-CH) $_{\text{Py}}$, 2H), 8.47–8.49 (dd, J_1 = 4.91 Hz, J_2 = 1.70 Hz, (C-CH-N-CH) $_{\text{Py}}$, 2H), 8.55–8.56 (d, J = 2.08 Hz, (C-CH-N) $_{\text{Py}}$, 2H). ^{13}C NMR (CDCl_3) δ 48.6 ($\text{O-CH}_2\text{-CH}_2\text{-N}$), 51.0 ($\text{CH}_2\text{-N}$), 70.2 ($\text{O-CH}_2\text{-CH}_2\text{-N}$), 70.4 (O-CH_2), 123.3 ((C-CH-CH) $_{\text{Py}}$), 135.6 ((C-CH-N) $_{\text{Py}}$), 135.7 ((C-CH-CH) $_{\text{Py}}$), 148.3 ((C-CH-N-CH) $_{\text{Py}}$), 149.6 ((C-CH-N) $_{\text{Py}}$). HR-MS (ESI): calculated for $\text{C}_{18}\text{H}_{27}\text{N}_4\text{O}_2^+$ m/z 331.2129 $\{M + H^+\}^+$, found 331.1953.

***N,N'*-(4-Pyridylmethyl)(ethylenedioxy)bis(ethylamine) (1_p).** The product was obtained as yellow oil in 91% yield. ^1H NMR (CDCl_3) δ 2.77–2.81 (t, J = 5.1 Hz, $\text{CH}_2\text{-NH}$, 4H), 3.60–3.62 (m, O-CH_2 , 8H), 3.81 (s, $\text{O-CH}_2\text{-CH}_2\text{-NH}$, 4H), 7.25–7.27 (d, J = 5.3 Hz, (C-CH) $_{\text{Py}}$, 4H), 8.51–8.53 (dd, J_1 = 4.53 Hz, J_2 = 1.51 Hz, (N-CH) $_{\text{Py}}$, 4H). ^{13}C NMR (CDCl_3) δ 48.7 ($\text{O-CH}_2\text{-CH}_2\text{-N}$), 52.5 ($\text{CH}_2\text{-N}$), 70.3 ($\text{O-CH}_2\text{-CH}_2\text{-N}$), 70.5 (O-CH_2), 122.9 (C-CH) $_{\text{Py}}$, 149.4 (C-CH) $_{\text{Py}}$, 149.7 (N-CH) $_{\text{Py}}$. HR-MS (ESI): calculated for $\text{C}_{18}\text{H}_{26}\text{N}_4\text{NaO}_2^+$ m/z 353.1948 $\{M + Na^+\}^+$, found 353.1953.

General procedure for alkylation of 1 to form 2

The flask containing diamine 1 (7.8 mmol) was flushed with nitrogen and dry DMF (40 mL) was added. Then potassium carbonate (62.6 mmol, 8 equiv.) and potassium iodide (4.7 mmol, 0.6 equiv.) were added under a stream of nitrogen. To the resulting mixture, *t*-butyl bromoacetate (31.3 mmol, 4 equiv.) was added dropwise in four portions. The flask was sealed with parafilm and left stirring at room temperature for 24 h. DMF was dried on a high-vacuum pump. The residue was dissolved in MeOH and dried with silica gel *in vacuo*. The derivatives 2_{o,m,p} were isolated using column chromatography on silica gel with gradient solvent mixtures: EtOAc/10% hexane, EtOAc, EtOAc + 1.5% EtOH.

***N,N'*-(*tert*-Butoxycarbonylmethyl)-*N,N'*-(2-pyridylmethyl)(ethylenedioxy)bis(ethylamine) (2_o).** The product was obtained as dark-red oil in 57% yield. ^1H NMR (CDCl_3) δ 1.46 (s, C-CH₃, 18H), 2.91–2.95 (t, J = 5.4 Hz, $\text{CH}_2\text{-N}$, 4H), 3.41 (s, CO-CH₂, 4H), 3.52–3.59 (m, O-CH_2 , 8H), 4.01 (s, $\text{O-CH}_2\text{-CH}_2\text{-N}$, 4H), 7.14–7.18 (t, J = 4.91 Hz, (C-CH-CH) $_{\text{Py}}$, 2H), 7.56–7.58 (d, J = 7.55 Hz, (C-CH-CH) $_{\text{Py}}$, 2H), 7.64–7.69 (t, J = 7.55 Hz, (N-CH-CH) $_{\text{Py}}$, 2H), 8.53–8.54 (d, J = 4.53 Hz, (N-CH-CH) $_{\text{Py}}$, 2H). ^{13}C NMR (CDCl_3) δ 28.2 (C-CH₃), 53.4 ($\text{O-CH}_2\text{-CH}_2\text{-N}$), 56.6 ($\text{CH}_2\text{-N}$), 60.4 (CO-CH₂), 69.9 ($\text{O-CH}_2\text{-CH}_2\text{-N}$), 70.2 (O-CH_2), 80.9 (C-CH₃), 122.0 ((N-CH-CH) $_{\text{Py}}$), 123.1 ((C-CH-CH) $_{\text{Py}}$), 136.7 ((C-CH-CH) $_{\text{Py}}$), 148.7 ((N-CH-CH) $_{\text{Py}}$), 159.6 ((CH-C-N) $_{\text{Py}}$), 170.7 (CO-CH₂). HR-MS (ESI): calculated for $\text{C}_{30}\text{H}_{46}\text{N}_4\text{NaO}_6^+$ m/z 581.3310 $\{M + Na^+\}^+$, found 581.3312.

***N,N'*-(*tert*-Butoxycarbonylmethyl)-*N,N'*-(3-pyridylmethyl)(ethylenedioxy)bis(ethylamine) (2_m).** The product was obtained as a dark-orange oil in 58% yield. ^1H NMR (CDCl_3) δ 1.46 (s, C-CH₃, 18H), 2.86–2.90 (t, J = 5.5 Hz, $\text{CH}_2\text{-N}$, 4H), 3.32 (s, CO-CH₂, 4H), 3.59 (s, O-CH_2 , 8H), 3.91 (s, $\text{O-CH}_2\text{-CH}_2\text{-N}$, 4H),

7.26–7.30 (dd, J_1 = 7.74 Hz, J_2 = 4.91 Hz, (C-CH-CH) $_{\text{Py}}$, 2H), 7.75–7.77 (d, J = 7.74 Hz, (C-CH-CH) $_{\text{Py}}$, 2H), 8.50–8.55 (m, (C-CH-N) $_{\text{Py}}$, (C-CH-N-CH) $_{\text{Py}}$, 4H). ^{13}C NMR (CDCl_3) δ 28.1 (C-CH₃), 53.2 ($\text{O-CH}_2\text{-CH}_2\text{-N}$), 55.8 (CO-CH₂), 55.9 ($\text{CH}_2\text{-N}$), 69.3 ($\text{O-CH}_2\text{-CH}_2\text{-N}$), 70.0 (O-CH_2), 81.3 (C-CH₃), 123.4 ((C-CH-CH) $_{\text{Py}}$), 134.0 ((C-CH-N) $_{\text{Py}}$), 137.1 ((C-CH-N) $_{\text{Py}}$), 148.4 ((C-CH-N-CH) $_{\text{Py}}$), 150.1 ((C-CH-CH) $_{\text{Py}}$), 171.0 (CO-CH₂). HR-MS (ESI): calculated for $\text{C}_{30}\text{H}_{46}\text{N}_4\text{NaO}_6^+$ m/z 581.3310 $\{M + Na^+\}^+$, found 581.3326.

***N,N'*-(*tert*-Butoxycarbonylmethyl)-*N,N'*-(4-pyridylmethyl)(ethylenedioxy)bis(ethylamine) (2_p).** The product was obtained as red oil in 65% yield. ^1H NMR (CDCl_3) δ 1.46 (s, C-CH₃, 18H), 2.86–2.90 (t, J = 5.7 Hz, $\text{CH}_2\text{-N}$, 4H), 3.32–3.35 (m, CO-CH₂, 4H), 3.54–3.60 (m, O-CH_2 , 8H), 3.88 (s, $\text{O-CH}_2\text{-CH}_2\text{-N}$, 4H), 7.32–7.34 (m, (C-CH) $_{\text{Py}}$, 4H), 8.51–8.53 (dd, J_1 = 4.53 Hz, J_2 = 1.51 Hz, (N-CH) $_{\text{Py}}$, 4H). ^{13}C NMR (CDCl_3) δ 28.1 (C-CH₃), 53.2 ($\text{O-CH}_2\text{-CH}_2\text{-N}$), 55.9 (CO-CH₂), 57.6 ($\text{CH}_2\text{-N}$), 70.0 ($\text{O-CH}_2\text{-CH}_2\text{-N}$), 70.2 (O-CH_2), 80.93 (C-CH₃), 123.6 (C-CH) $_{\text{Py}}$, 149.2 (C-CH) $_{\text{Py}}$, 149.3 (N-CH) $_{\text{Py}}$, 170.6 (CO-CH₂). HR-MS (ESI): calculated for $\text{C}_{30}\text{H}_{46}\text{N}_4\text{NaO}_6^+$ m/z 581.3310 $\{M + Na^+\}^+$, found 581.3311.

General procedure for acidic hydrolysis of 2 to form S₁

A solution of corresponding derivative 2 (0.48 mmol) in CH_2Cl_2 (6 mL) was flushed with nitrogen, cooled down in an ice-bath, and cold TFA (3.5 mL) was added dropwise. The progress of the reaction was monitored by mass spectrometry and TLC analysis. In the case of the diacid S_{1m}, an additional amount of TFA (0.5 mL) was required to complete the process. The solvents were removed using a rotary evaporator. MeOH was then added to the residue, and the solution was dried *in vacuo*. The procedure was repeated multiple times in order to remove the remaining TFA.

***N,N'*-(2-Pyridylmethyl)(ethylenedioxy)bis(ethylamine)-*N,N'*-diacetic acid (S_{1o}).** The product was obtained as dark-red sticky oil in 64% yield. ^1H NMR (D_2O) δ 3.43 (s, $\text{O-CH}_2\text{-CH}_2\text{-N}$, 4H), 3.57 (s, CO-CH₂, 4H), 3.76 (s, O-CH_2 , 8H), 4.50 (s, $\text{CH}_2\text{-Py}$, 4H), 7.41–7.48 (m, (C-CH-CH) $_{\text{Py}}$, (N-CH-CH) $_{\text{Py}}$, 4H), 7.83–7.88 (t, J = 7.74 Hz, (C-CH-CH) $_{\text{Py}}$, 2H), 8.52 (s, (N-CH-CH) $_{\text{Py}}$, 2H). ^{13}C NMR (CD_3OD) δ 55.5 ($\text{O-CH}_2\text{-CH}_2\text{-N}$), 57.9 ($\text{CH}_2\text{-N}$), 59.7 (CO-CH₂), 66.8 ($\text{O-CH}_2\text{-CH}_2\text{-N}$), 71.6 (O-CH_2), 125.3 ((N-CH-CH) $_{\text{Py}}$), 125.5 ((C-CH-CH) $_{\text{Py}}$), 139.2 ((C-CH-CH) $_{\text{Py}}$), 150.5 ((N-CH-CH) $_{\text{Py}}$), 152.7 ((CH-C-N) $_{\text{Py}}$), 170.7 (CO₂H). HR-MS (ESI): calculated for $\text{C}_{22}\text{H}_{31}\text{N}_4\text{O}_6^+$ m/z 447.2238 $\{M + H^+\}^+$, found 447.2243.

***N,N'*-(3-Pyridylmethyl)(ethylenedioxy)bis(ethylamine)-*N,N'*-diacetic acid (S_{1m}).** The product was crystallized as a protonated salt (as evidenced from NMR spectra) by slow diffusion of methanolic solution into Et₂O and isolated as a fine dark-red solid in 57% yield. ^1H NMR (CD_3OD) δ 3.33–3.35 (s, $\text{O-CH}_2\text{-CH}_2\text{-N}$, 4H), 3.66 (s, O-CH_2 , 4H), 3.80–3.83 (t, J = 4.53 Hz, $\text{O-CH}_2\text{-CH}_2\text{-N}$, 4H), 3.87 (s, CO-CH₂, 4H), 4.46 (s, $\text{CH}_2\text{-Py}$, 4H), 7.71–7.75 (dd, J_1 = 5.29 Hz, J_2 = 2.46 Hz, (C-CH-CH) $_{\text{Py}}$, 2H), 8.28–8.31 (d, J = 7.93 Hz, (C-CH-CH) $_{\text{Py}}$, 2H), 8.70–8.72 (d, J = 4.53 Hz, (C-CH-N-CH) $_{\text{Py}}$, 2H), 8.85 (s, (C-CH-N) $_{\text{Py}}$, 2H). ^{13}C NMR (CD_3OD) δ 55.0 ($\text{O-CH}_2\text{-CH}_2\text{-N}$), 55.6 (CO₂H-CH₂), 57.2



(CH₂-N), 67.8 (O-CH₂-CH₂-N), 71.3 (O-CH₂), 126.4 ((C-CH-CH)_{Py}), 132.9 ((C-CH-N)_{Py}), 143.3 ((C-CH-N)_{Py}), 148.2 ((C-CH-N-CH)_{Py}), 149.5 ((C-CH-CH)_{Py}), 171.3 (CO₂H). HR-MS (ESI): calculated for C₂₂H₃₁N₄O₆⁺ *m/z* 447.2238 {M + H⁺}⁺, found 447.2241.

***N,N'*-(4-Pyridylmethyl)(ethylenedioxy)bis(ethylamine)-*N,N'*-diacetic acid (S_{1p}).** The product was crystallized by slow diffusion of methanolic solution into Et₂O and isolated as dark-red solid in 43% yield. NMR (CD₃OD) δ 3.20 (s, O-CH₂-CH₂-N, 2H), 3.64–3.70 (m, CO-CH₂, O-CH₂, CH₂-Py, 8H), 3.75–3.79 (m, O-CH₂-CH₂-, O-CH₂-CH₂-NH⁺, CO-CH₂, 8H), 4.36 (s, NH⁺-CH₂-Py, 2H), 7.48–7.59 (m, (C-CH)_{Py}, 1H), 7.81 (s, (C-CH)_{Py}, 3H), 8.68 (s, (N-CH)_{Py}, 4H). ¹³C NMR (CD₃OD) δ 55.2 (O-CH₂-CH₂-N), 58.6 (CO₂H-CH₂), 59.7 (CH₂-N), 69.0 (O-CH₂-CH₂-N), 70.6 (O-CH₂), 126.1 (C-CH)_{Py}, 127.4 (C-CH)_{Py}, 150.1 (N-CH)_{Py}, 150.7 (C-CH)_{Py}, 179.1 (CO₂H). HR-MS (ESI): calculated for C₂₂H₃₁N₄O₆⁺ *m/z* 447.2238 {M + H⁺}⁺, found 447.2238.

Synthesis of ethylene glycol-bis(β-aminoethyl ether)-*N,N'*-diacetic-*N,N'*-dianhydride (EGTA-bis(anhydride)) (3). Prior to use ethylene glycol-bis(β-aminoethyl ether)-*N,N,N',N'*-tetraacetic acid (EGTA) was dried on a Schlenk line. A flask containing dry EGTA (0.5 g, 1.3 mmol) was filled with nitrogen, and freshly distilled dry pyridine (6 mL) was added *via* a septum. The mixture was purged with nitrogen for 15 min after which the flask was transferred to an oil bath and the temperature increased to 65 °C. To the resulting emulsion, acetic anhydride (0.5 mL, 5.3 mmol) was added dropwise slowly in 100 μL increments. The flask was sealed and stirring at 65 °C was continued for 24 h. After reaction completion (following the progress with mass analysis) the solvent was removed under reduced pressure. The product was obtained as a dark-brown oil in 91% yield. ¹H NMR (CDCl₃) δ 2.82–2.85 (t, *J* = 4.91 Hz, O-CH₂-CH₂-N, 4H), 3.58 (s, O-CH₂, 4H), 3.61–3.65 (t, *J* = 4.91 Hz, O-CH₂-CH₂-N, 4H), 3.69 (s, CO-CH₂, 8H). ¹³C NMR (CDCl₃) δ 53.6 (O-CH₂-CH₂-N), 54.9 (CO-CH₂), 69.2 (O-CH₂-CH₂-N), 70.3 (O-CH₂), 164.6 (CO-CH₂).

General procedure for the synthesis of S₂ derivatives

Into a Schlenk flask containing the anhydride **3** (0.5 g, 1.5 mmol), dry pyridine (4 mL) was added and the mixture was purged with nitrogen for 15 min. In a separate Schlenk flask a solution of the corresponding aminopyridine (0.3 g, 3.2 mmol) in 3–4 mL of dry solvent (pyridine or DMF) was prepared. Due to limited solubility of 4-aminopyridine in pyridine, DMF was used in this case. The resulting solution was added to the anhydride **3** *via* a rubber septum. The flask was sealed and left stirring under nitrogen for 14 h. The solvent was removed under reduced pressure. The residue was re-dissolved in water, the pH was adjusted to 10 and the mixture was washed with diethyl ether (4 × 30 mL). The aqueous fraction was dried under reduced pressure and the residue was purified by preparative HPLC.

***N,N'*-Bis[(3-pyridinyl)aminocarbonyl]-ethylene glycol-bis(β-aminoethyl ether)-*N,N'*-diacetic acid (S_{2m}).** S_{2m} was isolated using HPLC with a 5 min linear gradient from 2 to 20%

acetonitrile followed by a 30 min linear gradient from 20 to 50%. The product was obtained as a light-brown crystalline in 42% yield. ¹H NMR (D₂O) δ 2.62 (s, O-CH₂-CH₂-N, 4H), 3.15 (s, O-CH₂, 4H), 3.22–3.24 (d, *J* = 6.07 Hz, O-CH₂-CH₂-N, 4H), 3.35 (s, CO₂H-CH₂, CO-CH₂, 8H), 7.16–7.20 (q, *J*₁ = 4.91 Hz, *J*₂ = 3.40 Hz, (C-CH-CH)_{Py}, 2H), 7.72–7.75 (d, *J* = 8.31 Hz, (C-CH-N-CH)_{Py}, 2H), 8.06–8.08 (d, *J* = 4.72 Hz, (C-CH-CH)_{Py}, 2H), 8.41 (s, (C-CH-N)_{Py}, 2H). ¹³C NMR (D₂O) δ 54.5 (O-CH₂-CH₂-N), 59.2 (CO-CH₂), 59.4 (CO₂H-CH₂), 68.3 (O-CH₂-CH₂-N), 69.3 (O-CH₂), 124.3 ((C-CH-N)_{Py}), 128.6 ((C-CH-CH)_{Py}), 134.3 ((C-CH-N)_{Py}), 140.8 ((C-CH-N-CH)_{Py}), 144.6 ((C-CH-CH)_{Py}), 173.3 (CO-CH₂), 179.1 (CO₂H-CH₂). HR-MS (ESI): calculated for C₂₄H₃₂KN₆O₈⁺ *m/z* 571.1913 {M + K⁺}⁺, found 571.1825.

***N,N'*-Bis[(4-pyridinyl)aminocarbonyl]-ethylene glycol-bis(β-aminoethyl ether)-*N,N'*-diacetic acid (S_{2p}).** S_{2p} was isolated using HPLC with a 20 min linear gradient from 2 to 5% acetonitrile, followed by a 5 min linear gradient from 5 to 10% and, finally, 5 min linear gradient from 10 to 50%. The product was obtained as a light-yellow crystalline solid in 29% yield. ¹H NMR (D₂O) δ 3.03 (s, O-CH₂-CH₂-N, 4H), 3.48 (s, CO₂H-CH₂, CO-CH₂, 8H), 3.60 (s, O-CH₂, 4H), 3.74 (s, O-CH₂-CH₂-N, 4H), 7.74 (s, (CH-CH-N)_{Py}, 4H), 8.40 (s, (CH-CH-N)_{Py}, 4H). ¹³C NMR (D₂O) δ 55.1 (O-CH₂-CH₂-N), 59.0 (CO-CH₂), 59.2 (CO₂H-CH₂), 67.4 (O-CH₂-CH₂-N), 69.5 (O-CH₂), 114.8 ((CH-CH-N)_{Py}), 145.4 ((CH-CH-N)_{Py}), 149.0 ((C-CH)_{Py}), 171.5 (CO-CH₂), 176.0 (CO₂H-CH₂). HR-MS (ESI): calculated for C₂₄H₃₃N₆O₈⁺ *m/z* 533.2354 {M + H⁺}⁺, found 533.2358.

Synthesis of *N*-Boc-*N'*-(3-pyridylmethyl)-2,2-(ethylenedioxy)bis(ethylamine) (4). **4** was obtained in 90% yield from *tert*-butyl (2-(2-(2-aminoethoxy)ethoxy)ethyl)carbamate following the general procedure for reductive amination described above, adapted for mono-substitution. Thus, diethylamine (0.51 g, 2.1 mmol) and nicotinaldehyde (0.24 g, 2.2 mmol) were dissolved in dry CH₂Cl₂ (10 mL) and the solution was stirred under nitrogen for 18 h. After the work-up as described above for **1**, the residue was dissolved in absolute EtOH (10 mL), cooled down in an ice-bath and NaBH₄ (0.19 g, 5 mmol) was added in portions under a stream of nitrogen. After the work-up as described above for **1**, the product **4** was obtained as a light-yellow oil and used without further purification. ¹H NMR (CDCl₃) δ 1.44 (s, C-CH₃, 9H), 2.80–2.84 (t, *J* = 5.1 Hz, O-CH₂-CH₂-NH-CH₂-Py, 2H), 3.29–3.33 (m, CO-NH-CH₂, 2H), 3.52–3.55 (t, *J* = 5.1 Hz, O-CH₂-CH₂-NH, 2H), 3.61–3.65 (m, O-CH₂, 6H), 3.84 (s, Py-CH₂, 2H), 7.24–7.28 (dd, *J*₁ = 4.72 Hz, *J*₂ = 3.02 Hz, (C-CH-CH)_{Py}, 1H), 7.69–7.72 (d, *J* = 7.74 Hz, (C-CH-CH)_{Py}, 1H), 8.49–8.51 (d, *J* = 4.72 Hz, (C-CH-N-CH)_{Py}, 1H), 8.57 (d, *J* = 2.08 Hz, (C-CH-N)_{Py}, 1H). ¹³C NMR (CDCl₃) δ 28.4 (C-CH₃), 40.3 (CO-NH-CH₂), 48.5 (O-CH₂-CH₂-N), 51.0 (Py-CH₂), 70.2 (O-CH₂), 70.3 (O-CH₂-CH₂-N), 79.1 (C-CH₃), 123.4 ((C-CH-CH)_{Py}), 135.4 ((C-CH-N)_{Py}), 135.9 ((C-CH-CH)_{Py}), 148.4 ((C-CH-N-CH)_{Py}), 149.7 ((C-CH-N)_{Py}), 156.0 (CO). HR-MS (ESI): calculated for C₁₇H₃₀N₃O₄⁺ *m/z* 340.22308 {M + H⁺}⁺, found 340.22248.

***N*-[Boc-(*tert*-butoxycarbonyl)methyl]-*N'*-[(*tert*-butoxycarbonyl)methyl-(3-pyridylmethyl)]-2,2-(ethylenedioxy)bis(ethylamine) (5).** The alkylation was carried out following the general procedure



described above for preparation of **2**. The target derivative **5** was isolated using column chromatography on silica gel with gradient solvent mixtures: hexane/EtOAc (5/3, 1/1, 1/3), EtOAc, EtOAc + 1.5% MeOH in 73% yield. ^1H NMR (CDCl_3) δ 1.43–1.44 (d, J = 5.1 Hz, C-CH_3 , 18H), 1.47 (s, C-CH_3 , 9H), 2.88–2.92 (t, J = 5.67 Hz, $\text{O-CH}_2\text{-CH}_2\text{-N-CH}_2\text{-Py}$, 2H), 3.30–3.33 (m, CO-N-CH_2 , $\text{CO-CH}_2\text{-N-CH}_2\text{-Py}$, 4H), 3.51–3.53 (d, J = 5.29 Hz, $\text{O-CH}_2\text{-CH}_2\text{-N-CH}_2\text{-Py}$, 2H), 3.55–3.59 (m, O-CH_2 , 6H), 3.65 (s, $\text{CO-CH}_2\text{-N}$, 2H), 3.89 (s, Py-CH_2 , 2H), 7.24–7.28 (dd, J_1 = 4.91 Hz, J_2 = 3.02 Hz, $(\text{C-CH-CH})_{\text{Py}}$, 1H), 7.73–7.76 (d, J = 7.74 Hz, $(\text{C-CH-CH})_{\text{Py}}$, 1H), 8.50–8.51 (d, J = 3.59 Hz, $(\text{C-CH-N-CH})_{\text{Py}}$, 1H), 8.59 (s, $(\text{C-CH-N})_{\text{Py}}$, 1H). ^{13}C NMR (CDCl_3) δ 28.1 (C-CH_3), 28.4 (C-CH_3), 53.0 ($\text{O-CH}_2\text{-CH}_2\text{-N}$), 53.4 (Py-CH_2), 55.7 ($\text{CO-CH}_2\text{-N}$), 56.0 ($\text{O-CH}_2\text{-CH}_2\text{-N-CH}_2\text{-Py}$), 70.0 ($\text{O-CH}_2\text{-CH}_2\text{-N}$), 70.3 (O-CH_2), 81.1 (C-CH_3), 123.4 ($(\text{C-CH-CH})_{\text{Py}}$), 134.9 ($(\text{C-CH-N})_{\text{Py}}$), 136.7 ($(\text{C-CH-N})_{\text{Py}}$), 148.5 ($(\text{C-CH-N-CH})_{\text{Py}}$), 150.2 ($(\text{C-CH-CH})_{\text{Py}}$), 156.1 (CO), 170.7 (CO). HR-MS (ESI): fragments calculated for $\text{C}_{23}\text{H}_{44}\text{N}_2\text{O}_8$ m/z 476.3092 $\{\text{M} + \text{H}^+ - \text{PyCH}_2^+\}$, found 476.2733; calculated for $\text{C}_{23}\text{H}_{40}\text{N}_3\text{O}_6^+$ m/z 454.2912 $\{\text{M} + 2\text{H}^+ - \text{CH}_2\text{CO}_2^+\text{Bu}^+\}$, found 454.2914.

Synthesis of *N*-(formic acid)-*N'*-(3-pyridylmethyl)-2,2-(ethylenedioxy) bis(ethylamine)-*N,N'*-diacetic acid (S_{3m}**).** Starting compound **5** (0.64 g, 1.1 mM) was dissolved in dry dioxane (7 mL) in a flask filled with nitrogen. The mixture was cooled down in an ice bath and conc. HCl was added dropwise in 0.5 mL steps over 30 min (3 mL in total). After 20 min the ice bath was removed and the mixture was allowed to warm to room temperature and left stirring for 4 h. The solvent was then evaporated and the residue purified using HPLC with a 10 min linear gradient from 2 to 10% acetonitrile, followed by a 5 min linear gradient from 10 to 20%. The product **S_{3m}** was obtained as a dark-brown oil in 67% yield. ^1H NMR (D_2O) δ 2.83 (s, $\text{O-CH}_2\text{-CH}_2\text{-N-CH}_2\text{-Py}$, 2H), 2.99 (s, $\text{O-CH}_2\text{-CH}_2\text{-N}$, 2H), 3.28 (s, CO-CH_2 , 2H), 3.39 (m, CO-NH-CH_2 , 4H), 3.45 (s, CO-CH_2 , 2H), 3.58 (s, $\text{O-CH}_2\text{-CH}_2\text{-N-CH}_2\text{-Py}$, 2H), 3.65 (s, $\text{O-CH}_2\text{-CH}_2\text{-N}$, 2H), 3.90 (s, Py-CH_2 , 2H), 7.85 (m, $(\text{C-CH-CH})_{\text{Py}}$, 1H), 8.49–8.52 (d, J = 7.37 Hz, $(\text{C-CH-CH})_{\text{Py}}$, 1H), 8.59 (s, $(\text{C-CH-N-CH})_{\text{Py}}$, 1H), 8.73 (s, $(\text{C-CH-N})_{\text{Py}}$, 1H). ^{13}C NMR (D_2O) δ 39.0 ($\text{O-CH}_2\text{-CH}_2\text{-N}$), 46.8 ($\text{N-CH}_2\text{-CO}_2\text{H}$), 47.3 ($\text{CO-NH}^+-\text{CH}_2$), 54.2 ($\text{O-CH}_2\text{-CH}_2\text{-N-CH}_2\text{-Py}$), 55.0 ($\text{CO}_2\text{H-CH}_2\text{-N-CH}_2\text{-Py}$), 64.2 (Py-CH_2), 65.1 ($\text{O-CH}_2\text{-CH}_2\text{-N}$), 66.1 ($\text{O-CH}_2\text{-CH}_2\text{-N-CH}_2\text{-Py}$), 69.3 (O-CH_2), 128.0 ($(\text{C-CH-CH})_{\text{Py}}$), 128.9 ($(\text{C-CH-N})_{\text{Py}}$), 142.7 ($(\text{C-CH-N})_{\text{Py}}$), 143.5 ($(\text{C-CH-N-CH})_{\text{Py}}$), 150.0 ($(\text{C-CH-CH})_{\text{Py}}$), 168.1 (NH^+-CO), 168.6 (CO_2H). HR-MS (ESI): calculated for $\text{C}_{17}\text{H}_{22}\text{N}_3\text{O}_7^{2-}$ m/z 380.3736 $\{\text{M} - 2\text{H} - \text{OH}\}^{2-}$, found 380.7067.

SABRE procedures

Parahydrogen (pH_2) was produced by passing hydrogen gas over a spin-exchange catalyst (Fe_2O_3) and used for all hyperpolarisation experiments. This method produces constant pH_2 with ca. 98% purity. ^1H (400 MHz) and ^{13}C (100.6 MHz) NMR spectra were recorded with an internal deuterium lock. Chemical shifts are quoted as parts per million and referenced

to the solvent. ^{13}C NMR spectra were recorded with broadband proton decoupling. Coupling constants (J) are quoted in Hertz.

Samples were prepared in a 5 mm NMR tube that was fitted with a J. Young's tap. $[\text{IrCl}(\text{COD})(\text{IMes})]$ was synthesized according to a literature procedure.⁵⁹ The resulting solutions were degassed by two freeze-pump-thaw cycles before the addition of 3-bar H_2 .

The shake and drop method was employed for recording hyperpolarised NMR spectra. This involves filling NMR tubes with pH_2 at 3 bar pressure and shaking them vigorously for 10 seconds in a 65 G magnetic field (stray field of the 9.4 T spectrometer). Typically, three shake and drop measurements are recorded and average ^1H NMR signal enhancement values are quoted. The typical variation among these measurements is $\leq \pm 10\%$. Signal enhancements are calculated by dividing the integrated signal intensities from a single scan hyperpolarised spectrum by its thermal counterpart recorded under the same spectral conditions. These values are presented per fold, *i.e.* a 100-fold enhancement means that hyperpolarised signals are 100 times more intense than those recorded using Boltzmann controlled NMR.

Author contributions

Ben. J. Tickner: conceptualization, methodology, investigation (SABRE measurements), writing – original draft, visualization. Yulia Borozdina: investigation (Agent synthesis), writing – original draft. Simon B. Duckett: methodology, writing – review & editing, supervision, funding acquisition. Goran Angelowski: conceptualization, methodology, writing – review & editing, visualization, supervision, funding acquisition.

Conflicts of interest

The authors have no conflicts to declare.

Acknowledgements

We thank Dr Peter Rayner and Dr Victoria Annis for synthesis of the iridium precatalysts and Dr Marianna Fekete for helpful discussions. Financial support from the Wellcome Trust (Grants 092506 and 098335), the MRC (MR/M008991/1), the EPSRC (B. J. T. studentship) and the Shanghai Municipal Science and Technology Major Project (Grant No. 2019SHZDZX02) is gratefully acknowledged. Open Access funding provided by the Max Planck Society.

References

- 1 J. Wahsner, E. M. Gale, A. Rodríguez-Rodríguez and P. Caravan, *Chem. Rev.*, 2019, **119**, 957–1057.
- 2 D. V. Hingorani, A. S. Bernstein and M. D. Pagel, *Contrast Media Mol. Imaging*, 2015, **10**, 245–265.



- 3 G. Angelovski, *Angew. Chem., Int. Ed.*, 2016, **55**, 7038–7046.
- 4 N. K. Logothetis, *Nature*, 2008, **453**, 869–878.
- 5 B. Wu, G. Warnock, M. Zaiss, C. Lin, M. Chen, Z. Zhou, L. Mu, D. Nanz, R. Tuura and G. Delso, *EJNMMI Phys.*, 2016, **3**, 19.
- 6 E. L. Que and C. J. Chang, *Chem. Soc. Rev.*, 2010, **39**, 51–60.
- 7 G. Angelovski and É. Tóth, *Chem. Soc. Rev.*, 2017, **46**, 324–336.
- 8 P. Caravan, *Acc. Chem. Res.*, 2009, **42**, 851–862.
- 9 G. G. Somjen, *Ions in the brain : normal function, seizures, and strokes*, Oxford University Press, New York; Oxford, 2004.
- 10 H. Li and T. J. Meade, *J. Am. Chem. Soc.*, 2019, **141**, 17025–17041.
- 11 G. Angelovski, *Acc. Chem. Res.*, 2017, **50**, 2215–2224.
- 12 W.-H. Li, G. Parigi, M. Fragai, C. Luchinat and T. J. Meade, *Inorg. Chem.*, 2002, **41**, 4018–4024.
- 13 P. Nikolaou, B. M. Goodson and E. Y. Chekmenev, *Chem. – Eur. J.*, 2015, **21**, 3156–3166.
- 14 J. H. Ardenkjær-Larsen, S. Bowen, J. R. Petersen, O. Rybalko, M. S. Vinding, M. Ullisch and N. C. Nielsen, *Magn. Reson. Med.*, 2019, **81**, 2184–2194.
- 15 S. J. Nelson, J. Kurhanewicz, D. B. Vigneron, P. E. Z. Larson, A. L. Harzstark, M. Ferrone, M. Van Criekinge, J. W. Chang, R. Bok and I. Park, *Sci. Transl. Med.*, 2013, **5**, 198ra108–198ra108.
- 16 J. B. Hövener, A. N. Pravdivtsev, B. Kidd, C. R. Bowers, S. Glöggler, K. V. Kovtunov, M. Plaumann, R. Katz-Brull, K. Buckenmaier and A. Jerschow, *Angew. Chem., Int. Ed.*, 2018, **57**, 11140–11162.
- 17 D. Canet, C. Aroulanda, P. Mutzenhardt, S. Aime, R. Gobetto and F. Reineri, *Concepts Magn. Reson., Part A*, 2006, **28**, 321–330.
- 18 R. W. Adams, J. A. Aguilar, K. D. Atkinson, M. J. Cowley, P. I. Elliott, S. B. Duckett, G. G. Green, I. G. Khazal, J. López-Serrano and D. C. Williamson, *Science*, 2009, **323**, 1708–1711.
- 19 W. Iali, S. S. Roy, B. J. Tickner, F. Ahwal, A. J. Kennerley and S. B. Duckett, *Angew. Chem.*, 2019, **131**, 10377–10381.
- 20 T. Theis, M. L. Truong, A. M. Coffey, R. V. Shchepin, K. W. Waddell, F. Shi, B. M. Goodson, W. S. Warren and E. Y. Chekmenev, *J. Am. Chem. Soc.*, 2015, **137**, 1404–1407.
- 21 P. J. Rayner, P. Norcott, K. M. Appleby, W. Iali, R. O. John, S. J. Hart, A. C. Whitwood and S. B. Duckett, *Nat. Commun.*, 2018, **9**, 4251.
- 22 P. J. Rayner, M. J. Burns, A. M. Olaru, P. Norcott, M. Fekete, G. G. R. Green, L. A. R. Highton, R. E. Mewis and S. B. Duckett, *Proc. Natl. Acad. Sci. U. S. A.*, 2017, **114**, E3188–E3194.
- 23 D. A. Barskiy, S. Knecht, A. V. Yurkovskaya and K. L. Ivanov, *Prog. Nucl. Magn. Reson. Spectrosc.*, 2019, **114**, 33–70.
- 24 D. A. Barskiy, A. N. Pravdivtsev, K. L. Ivanov, K. V. Kovtunov and I. V. Koptug, *Phys. Chem. Chem. Phys.*, 2016, **18**, 89–93.
- 25 D. A. Barskiy, R. V. Shchepin, C. P. N. Tanner, J. F. P. Colell, B. M. Goodson, T. Theis, W. S. Warren and E. Y. Chekmenev, *ChemPhysChem*, 2017, **18**, 1493–1498.
- 26 M. Fekete, F. Ahwal and S. B. Duckett, *J. Phys. Chem. B*, 2020, **124**, 4573–4580.
- 27 R. E. Mewis, R. A. Green, M. C. Cockett, M. J. Cowley, S. B. Duckett, G. G. Green, R. O. John, P. J. Rayner and D. C. Williamson, *J. Phys. Chem. B*, 2015, **119**, 1416–1424.
- 28 W. Iali, P. J. Rayner, A. Alshehri, A. J. Holmes, A. J. Ruddlesden and S. B. Duckett, *Chem. Sci.*, 2018, **9**, 3677–3684.
- 29 M. Gemeinhardt, M. Limbach, T. Gebhardt, C. Eriksson, S. Eriksson, J. Lindale, E. Goodson, W. Warren, E. Chekmenev and B. Goodson, *Angew. Chem.*, 2020, **132**, 426–431.
- 30 P. J. Rayner, B. J. Tickner, W. Iali, M. Fekete, A. D. Robinson and S. B. Duckett, *Chem. Sci.*, 2019, **10**, 7709–7717.
- 31 P. M. Richardson, W. Iali, S. S. Roy, P. J. Rayner, M. E. Halse and S. B. Duckett, *Chem. Sci.*, 2019, **10**, 10607–10619.
- 32 P. J. Rayner, P. M. Richardson and S. B. Duckett, *Angew. Chem.*, 2020, **132**, 2732–2736.
- 33 A. M. Olaru, M. J. Burns, G. G. R. Green and S. B. Duckett, *Chem. Sci.*, 2017, **8**, 2257–2266.
- 34 R. V. Shchepin, D. A. Barskiy, A. M. Coffey, T. Theis, F. Shi, W. S. Warren, B. M. Goodson and E. Y. Chekmenev, *ACS Sens.*, 2016, **1**, 640–644.
- 35 F. F. Diaz-Rullo, F. Zamberlan, R. E. Mewis, M. Fekete, L. Broche, L. A. Cheyne, S. Dall'Angelo, S. B. Duckett, D. Dawson and M. Zanda, *Bioorg. Med. Chem.*, 2017, **25**, 2730–2742.
- 36 B. J. Tickner, P. J. Rayner and S. B. Duckett, *Anal. Chem.*, 2020, **92**, 9095–9103.
- 37 A. Mishra, G. Pariani, T. Oerther, M. Schwaiger and G. G. Westmeyer, *Anal. Chem.*, 2016, **88**, 10790–10794.
- 38 M. Naraghi, *Cell Calcium*, 1997, **22**, 255–268.
- 39 R. Hata, H. Nonaka, Y. Takakusagi, K. Ichikawa and S. Sando, *Chem. Commun.*, 2015, **51**, 12290–12292.
- 40 H. Nonaka, R. Hata, T. Doura, T. Nishihara, K. Kumagai, M. Akakabe, M. Tsuda, K. Ichikawa and S. Sando, *Nat. Commun.*, 2013, **4**, 2441.
- 41 T. B. R. Robertson, L. H. Antonides, N. Gilbert, S. L. Benjamin, S. K. Langley, L. J. Munro, O. B. Sutcliffe and R. E. Mewis, *ChemistryOpen*, 2019, **8**, 1375–1382.
- 42 T. Ratajczyk, T. Gutmann, P. Bernatowicz, G. Buntkowsky, J. Frydel and B. Fedorczyk, *Chem. – Eur. J.*, 2015, **21**, 12616–12619.
- 43 C. M. Wong, M. Fekete, R. Nelson-Forde, M. R. D. Gatus, P. J. Rayner, A. C. Whitwood, S. B. Duckett and B. A. Messerle, *Catal. Sci. Technol.*, 2018, **8**, 4925–4933.
- 44 S. Aime, A. Barge, M. Botta, L. Frullano, U. Merlo and K. I. Hardcastle, *J. Chem. Soc., Dalton Trans.*, 2000, 3435–3440.



- 45 T. S. Grimes, C. R. Heathman, S. Jansone-Popova, A. S. Ivanov, S. Roy, V. S. Bryantsev and P. R. Zalupski, *Inorg. Chem.*, 2018, **57**, 1373–1385.
- 46 S. Glöggler, R. Müller, J. Colell, M. Emondts, M. Dabrowski, B. Blümich and S. Appelt, *Phys. Chem. Chem. Phys.*, 2011, **13**, 13759–13764.
- 47 B. J. Tickner, W. Iali, S. S. Roy, A. C. Whitwood and S. B. Duckett, *ChemPhysChem*, 2019, **20**, 241–245.
- 48 B. J. Tickner, R. R. Parker, A. C. Whitwood and S. B. Duckett, *Organometallics*, 2019, **38**, 4377–4382.
- 49 S. Knecht, S. Hadjiali, D. A. Barskiy, A. Pines, G. Sauer, A. S. Kiryutin, K. L. Ivanov, A. V. Yurkovskaya and G. Buntkowsky, *J. Phys. Chem. C*, 2019, **123**, 16288–16293.
- 50 J. Colell, A. W. J. Logan, Z. Zhou, J. R. Lindale, R. Laasner, R. Shchepin, E. Chekmenev, V. Blum, W. S. Warren and S. J. Malcolmson, *Chem. Commun.*, 2020, **56**, 9336–9339.
- 51 C. P. N. Tanner, J. R. Lindale, S. L. Eriksson, Z. Zhou, J. F. P. Colell, T. Theis and W. S. Warren, *J. Chem. Phys.*, 2019, **151**, 044201.
- 52 B. J. Tickner, R. O. John, S. S. Roy, S. J. Hart, A. C. Whitwood and S. B. Duckett, *Chem. Sci.*, 2019, **10**, 5235–5245.
- 53 B. J. Tickner, O. Semenova, W. Iali, P. J. Rayner, A. C. Whitwood and S. B. Duckett, *Catal. Sci. Technol.*, 2020, **10**, 1343–1355.
- 54 B. J. A. van Weerdenburg, S. Glöggler, N. Eshuis, A. H. J. Engwerda, J. M. M. Smits, R. de Gelder, S. Appelt, S. S. Wymenga, M. Tessari and M. C. Feiters, *Chem. Commun.*, 2013, **49**, 7388–7390.
- 55 D. A. Barskiy, L. A. Ke, X. Li, V. Stevenson, N. Widarman, H. Zhang, A. Truxal and A. Pines, *J. Phys. Chem. Lett.*, 2018, **9**, 2721–2724.
- 56 W. Iali, A. M. Olaru, G. R. R. Green and S. B. Duckett, *Chem. – Eur. J.*, 2017, **23**, 10491–10495.
- 57 P. Spannring, I. Reile, M. Emondts, P. P. M. Schleker, N. K. J. Hermkens, N. G. J. van der Zwaluw, B. J. A. van Weerdenburg, P. Tinnemans, M. Tessari, B. Blumich, F. P. J. T. Rutjes and M. C. Feiters, *Chem. – Eur. J.*, 2016, **22**, 9277–9282.
- 58 M. Šebelaa, K. Jarkovská, R. Lenobelb, R. Meddac, A. Padigliac, G. Floris and P. Peča, *ARKIVOC*, 2007, **7**, 222–232.
- 59 L. D. Vazquez-Serrano, B. T. Owens and J. M. Buriak, *Inorg. Chim. Acta*, 2006, **359**, 2786–2797.

